universität wien

MASTERARBEIT / MASTER´S THESIS

Titel der Masterarbeit / Title of the Master´s Thesis

“Dissolution of Depleted Uranium Ammunition Corrosion Products”

verfasst von / submitted by

Sebastian Pontz BSc

angestrebter akademischer Grad / In partial fulfilment of the requirements for the degree of

Master of Science (MSc)

Wien, 2018 / Vienna, 2018

Studienkennzahl lt. Studienblatt / degree programme code as it appears on the student record sheet:	A 066 815
Studienrichtung lt. Studienblatt / degree programme as it appears on the student record sheet:	Masterstudium Erdwissenschaften
Betreut von / Supervisor:	Prof. Dr. Stephan Kraemer
Mitbetreut von / Co-Supervisor:	Dr. Walter Schenkeveld

Acknowledgements

First of all I would like to thank my Supervisors Prof.Dr. Krämer and Dr. Schenkeveld who gave me the opportunity to do my Master´s thesis at the University of Vienna in the department for geochemistry. They supported me during my work in the laboratory and were always open for scientific questions and discussions.

Special thanks go to Michael Ottman and Kyounglim Kang who performed the analysis with the ICP-MS. I also would like to thank Danielle Rushworth and Herwig Supper for their support in the laboratory.

Special thanks also go to Hugh, Klaudia and Katherina for their supporting reviews.

I would like to thank my friends who made the time at the university unforgettable, Johann, Max, Max, Marina, Simon, Philipp, Gerhard, Jakob and Sebastian.

I would like to express my gratitude to my parents for their endless support and encouragements during my studies. I am also very grateful to my sister and brother and my grandparents for their support.

Abstract

Depleted uranium (DU) is used in modern military conflicts as an ammunition. Most of the munition (90%) miss their targets and bury themselves in the ground, where the DU material is subjected to several weathering processes. Corrosion, dissolution and transport are the main processes controlling the mobility of the DU corrosion product and its potential impact to the environment. This thesis focuses on the dissolution process of the DU corrosion products. Two experimental set-ups have been performed. In batch experiments, the effect of different environmental conditions such as pH, pCO_2, salinity and organic ligands on the dissolution of DU have been tested. The results show that dissolution rate is increased at both acidic- (pH 3-4.5) and alkaline (pH 9) conditions. High CO_2 partial pressure as well as oxalic acid showed strongly supporting effects on the dissolution rate of uranium. The second experiment was performed using a continuous-flow stirred-tank reactor set-up in which dissolution products are removed from the system and the influence of the solution saturation state on the dissolution rate can be determined. The results show that the dissolution rate of DU is influenced by the solution saturation state. Increased solution saturation state has led to a slowdown of the dissolution rate. In summary, the dissolution of DU corrosion products was shown to be dependent on varying environmental parameters. These findings could be used for risk assessment in order to identify and distinguish risky soil from unproblematic soils in the context of DU dissolution.

Contents

List of figures

List of tables

1 Introduction

1.1 Depleted Uranium - general aspects

Uranium occurs predominantly in the minerals pitchblende and uraninite. There exist three different uranium isotopes (^{234}U, ^{235}U, and ^{238}U) in nature. 99.27% of ^{238}U, 0.72% of ^{235}U and 0.0054% of ^{234}U is the distribution of these isotopes in the continental crust (Bem and Bou-Rabee, 2004; Keith et.al. 2015). The isotope ^{235}U is due to its high radioactivity the most useful and attractive species as fuel for nuclear power plants. For the production of fuel with an increased amount of the ^{235}U isotope, the uranium undergoes an enrichment process. In enriched uranium the ^{235}U proportion is increased from 0.72% up to 3%-5% by mass (Upson, 1996).

During the enrichment process, uranium in which the isotope ^{235}U is depleted, is generated as a by-product. During the production of 1kg of enriched uranium fuel with 3% of ^{235}U, 5 kg of depleted uranium (DU) are produced (Bem and Bou-Rabee, 2004).The depletion of ^{235}U from 0.72% to 0.2% leads to a decrease in radioactivity of about 40% in DU as compared with natural uranium (WHO, 2001; Jiang & Aschner, 2015).

As a by-product, DU is easily available and cheap. The use of DU is widespread, and ranges from the use as counterweight in airplanes and as shielding in radiation therapy to military uses. Physical properties such as its high density, (19.07 g/cm^3) and its pyrophoric property (self-igniting when powdered) make depleted uranium attractive for military purposes. It can be used for defensive purposes like the reinforcement of military vehicles, such as tanks (Keith, 2015). It is also used as ammunition to penetrate armour plate. NATO airforces have fired DU munitions from A-10 antitank aircraft. Overall the use of DU in penetrators has been observed in many military conflicts in recent decades, including the first Gulf War in 1991, the conflict in Bosnia and Herzegovina in 1995, and the Serbia/Kosovo conflict in 1999. In total these conflicts have led to consumption and expose of many tons of DU (Bleise, et.al., 2003).During the 1991 gulf war alone 300 tons of DU were used (Bem and Bou-Rabee, 2004).

As a heavy metal, uranium affects human´s health through its chemical and radiological toxicity, targeting mainly the kidneys and the lung (WHO, 2001). Following the widespread use of DU in military conflicts and the consequent exposure of the environment to uranium, studies have been performed on the general risk and health effects of depleted uranium. There are several studies investigating the chemical and radiological toxicity and health effects of uranium (Keith, 2015; Jiang and Aschner, 2015; WHO, 2001; M.C. Thorne, J. Wilson 2001). However in DU, where the most radioactive uranium isotope ^{235}U is depleted, so that the level of radioactivity is reduced to 60% of that in natural uranium, the health risk to humans is derived from the chemical toxicity rather than from the radiological toxicity. Human`s exposure to uranium derived from a DU penetrator is possible in numerous ways. When a DU penetrator hits its target, the pyrophoric properties of uranium generate enormous heat whereby the uranium is vaporized, which leads to the release of up to 35% of the uranium as aerosols and fine dust into the air (Wang et.al. 2013). Intake through inhalation is a potential risk in such affected areas.

Up to 90% of penetrators miss their target, hit the ground and impact the environment. Weathering processes occurring in the soil can lead to corrosion of the metallic uranium and support the spread and migration of uranium in the environment. Uranium migration can eventually lead to contamination of ground water. Incorporation of uranium into the food chain is one possible scenario (Papastefanou, 2002). Uranium exposed in the soil is subject to a number of processes which cause risk of further exposure. Soil properties such as the redox potential, pH and salinity may affect the fate of DU in the environment.

1.2 Environmental fate of DU

There are two main ways in which DU impacts the environment. Either the DU penetrator hits the ground directly and stays in the soil or DU-aerosols and fine dust generated by a DU penetrator hitting a tank or comparable target are transported through air and settle to the ground. Whichever way the DU enters the environment, weathering processes take place and influence its fate. DU penetrators are composed of metallic uranium U(0) (Fomina, 2008). Once the DU has entered the soil, it is exposed to weathering processes, including corrosion. Corrosion leads to the formation of mixtures of secondary phases that include U in a more oxidized state (U(VI)). Under oxic conditions oxyhydroxide minerals, such as schoepite ($(UO_2)_8O_2(OH)_{12}*12H_2O$) and metaschoepite ($(UO_2)_4O(OH)_6*5H_2O$) can form (Reinoso-Maset, 2017). The corrosion reactions can be written as two simplified equations (eqs.1,2). First the metallic uranium reacts with oxygen derived from soil water and soil gas and is transformed to uraninite (UO_2)

$$U_{(s)} + O_2 \rightarrow UO_{2\,(s)} \qquad (1)$$

Still under oxic conditions the uraninite is transformed to a U(VI)-oxyhydroxide phase (metaschoepite)

$$UO_{2\,(s)} + ½\ O_2 + 2H_2O \rightarrow UO_3 \cdot 2H_2O_{(s)} \qquad (2)$$

In low O2 environments the corrosion reaction leads only to the formation of uraninite (UO_2) (eq.3) (Handley-Sidhu, 2008).

$$U_{(s)} + 2H_2O \rightarrow UO_{2\,(s)} + 2H_2 \qquad (3)$$

Once the corrosion products are formed dissolution reactions may take place. Uranium occurs naturally in two oxidation states (U(IV) and U(VI)). Dissolution is dependent on the solubility of the different uranium species. U(VI) species are more soluble than U(IV) species. While the stable uraninite stays mainly as solid, the uranium oxyhydroxides such as schoepite and metaschoepite dissolve under the right conditions (eq.4) (Giammar, 2001).

$$UO_3 \cdot 2H_2O_{(s)} + 2H^+ \rightarrow UO_2^{2+}{}_{(aq)} + 3H_2O \qquad (4)$$

Once the uranium is in solution it occurs as uranyl ion (UO_2^{2+}). In solution, there are several processes influencing further transport. A change in redox potential may lead to precipitation. Adsorption properties of the soil may also play a role controlling the mobility.

1.3 Solubility of uranium minerals

Environmental parameters like the redox potential are able to control the speciation of uranium phases. The main oxidation stages of uranium are U(VI) and U(IV). Different uranium species show, depending on their oxidation stage, varying solubility constants. U(IV) forms minerals such as uraninite (UO_2). Uraninite and other U(IV) phases are principally known as insoluble phases (Casas, 1998). The main U(VI) minerals occurring naturally are schoepite and metaschoepite, both of which are characterized by the higher solubility regarding to U(IV) species. The solubility of metaschoepite for example is found to be lg K_{sp}=4.68 (±0.14) to 6.59 (±0.14) regarding to equation 5 (Gorman-Lewis, 2008).

$2H^+ + UO_3(H_2O)_2 = UO_2^{2+} + 3H_2O$. (5)

As shown by Wang (2016) the DU corrosion products used in this study, consist mainly metaschoepite, studtite and becquelerite. Becquelerite (eq. 6) shows a solubility of lg K_{sp}=41.2-44.17, which is even more soluble than metaschoepite.

$14H^+ + Ca(UO_2)_6O_4(OH)_6(H_2O)_8 = Ca^{2+} + 6UO_2^{2+} + 18H_2O$ (6)

Studtite (eq.7) has a solubility of lg K_{sp}=-2.88 to -2.86, which is less soluble than metaschoepite (Gorman-Lewis, 2008).

$UO_2O_2(H_2O)_4 + 2H^+ = UO_2^{2+} + H_2O_2 + 4H_2O$ (7)

Therefore it can be summarized, that the three main U(VI) minerals of DU corrosion products, used here have major differences in their solubility and form thus a highly diverse mineral group. Due to this diversity, the dissolution properties of DU corrosion products are of high relevance and interest in this study.

1.4 Dissolution of DU corrosion products under various environmental conditions

The main mineralogical component in the DU corrosion product used here was characterized by the group of Prof. Bernier-Latmani as metaschoepite with additional becquerelite and studtite. The dissolution rates of U(VI) bearing minerals has been investigated by a number of researchers (Pérez, 1996, S. Steward, 1996, Pérez I. I., 2000, Giammar, 2002 , Reinoso-Maset, 2017, Wang G. W.-M., 2017). Liu et al. (2004) studied the dissolution rates of uranyl silicate micro precipitates in sediments at the Hanford site.

The dissolution mechanisms of metal oxides include proton-promoted dissolution, alkaline dissolution and ligand-controlled dissolution (Furrer, 1986; Wieland, 1988). It is typically assumed that the overall dissolution rate is the sum of the rates of these three mechanisms:

$$R = R_H + R_{OH} + R_L \qquad (8)$$

Where R is the overall dissolution rate, R_H, R_{OH}, and R_L, are the rates of proton-promoted-, alkaline-, and ligand-controlled dissolution, respectively. All these are considered surface controlled mechanisms, where the rates depend on the surface speciation of the dissolving mineral. Proton promoted dissolution depends on the protonation of surface sites and therefore tends to be high at low pH, alkaline dissolution depends on the de-protonation of surface sites and accelerates at high pH. Ligand promoted dissolution increases with increasing adsorption of ligands and the formation of inner sphere metal-ligand surface complexes. A fourth dissolution mechanism is the reductive or oxidative dissolution where the dissolution mechanism involves a change of redox-state of a component of the mineral. The oxidative dissolution of uraninite (UO_2) in the presence of oxygen or other electron acceptors are examples of this mechanism (Wang, 2014).

Dissolution rates of metal oxides decrease as solubility equilibrium is reached between the solution and the dissolving mineral phase reaction (Kraemer, 1997). This effect can be quantified by transition state theory derived rate laws, calculating a net dissolution rate that is affected by the forward dissolution rate and its back reaction. At equilibrium, the forward

and backward rates are equal. Such rate laws only correctly describe the effect of solution saturation state on observed dissolution rates as long as no secondary precipitates form (Giammar, 2002).

The dissolution of a mineral-oxide is controlled by the pH and the presence of inorganic and organic ligands derived from solution. One inorganic ligand known for its strong affinity for uranyl is carbonate. Carbonate in soil-solution derives from atmospheric CO_2 with a partial pressure of pCO2=-3.5 or CO_2 in soil-gas, which can be found in even higher concentrations. In the presence of dissolved carbonate species, e.g. in equilibrium with carbonaceous minerals and a carbon dioxide-containing atmosphere, uranium dissolution may be supported and stable carbonate complexes can form. This process can even be supported by a pH increase when bicarbonate deprotonates to carbonate. Previous studies on this topic prove that the presence of carbonate in solution has a strong effect on dissolution rates (Pérez I. I., 1996, S. Steward, 1996, Pérez I. I., 2000, Giammar, 2002, Reinoso-Maset, 2017, Wang G. W.-M., 2017). Based on comparison between a transition state theory derived rate law and the observed effect of carbonate, Reinoso-Maset et al. (2017) concluded that carbonate accelerates dissolution of a layered uranyl oxohydroxide by a ligand controlled mechanism. At low carbonate dissolution they suggested that a surface controlled mechanism such as proton promoted dissolution controls dissolution rates with the detachment of uranyl from the surface being rate-determining. U(VI)-carbonate complexes are quite stable and provide the potential for uranium transport through soils, sediments and aquifers.

Organic ligands such as humic acid (HA) and oxalate, both present in soil, are known to influence dissolution rates. There are several studies on the uranyl binding property of natural organic matter (NOM) (W. C. Li, 1980, Hummel, 1998). Humic acid is an organic ligand composed of various functional groups with mineral surface binding properties and is therefore of high interest in dissolution studies of DU corrosion products (W. C. Li, 1980).

1.5 Objectives

A depleted uranium penetrator exposed to the environment has the potential risk of uranium contaminating drinking water and entering the food chain (WHO, 2001). Processes like corrosion and oxidation form DU corrosion products, mainly U(VI) bearing oxyhydroxides. Dissolution and transport processes influence the mobility of uranium in soil. The corrosion of DU has been studied by Lathmani and Wang (2014). For pure uranium (VI) phases, dissolution rates under varying environmental parameters has been reported (Giammar D.E. 2001, Riba et.al. 2005, Gorman-Lewis 2008). The rate at which DU corrosion products dissolve has hardly been studied but is highly dependent on surface mechanisms, influenced by different solution compositions. As part of a broader investigation into the mobility of DU in soils, this study deals with the dissolution rate of DU corrosion products under a range of environmental conditions. The dissolution rate is the rate at which a certain amount of solid is dissolved over time, expressed as $\mu mol\ m^{-2}\ h^{-1}$. One goal of this study was to find out, in which range the dissolution rates of DU corrosion products vary within different solution compositions, regarding specific surface dissolution mechanisms (e.g. ligand-promoted dissolution). Another goal is to see the effect of the solution saturation state on dissolution rates.

Therefore two experimental set ups were conducted. Environmental parameters such as pH, salinity, CO_2 partial pressure, suspension density, and the presence of organic ligands have been simulated in batch experiments. The effect of the solution saturation state on the dissolution of DU corrosion products has been investigated in a continuous flow stirred tank reactor (CFSTR).

2 Materials and methods

2.1 Materials

The material studied, consists of scrapings from a DU penetrator which was collected by the UNEP and Spiez Laboratory in Bosnia Herzegovina in the vicinity of the Hadzici Tank Repair facility between October 12 and 24, 2002. The penetrator had been found embedded in a soil-cement mixture and has been referred to in the UNEP report as: “NUC-02-024-401” in the UNEP report. The penetrator was transported to the Spiez Laboratory where it was cleaned. Corrosion products from the DU penetrator were collected in 3 batches; an outer layer, directly in contact with the environment, an inner layer directly on top of the metallic uranium core, and an intermediate layer in between. The material used for the dissolution experiments corresponds with corrosion products from the intermediate layer (DUCP-Hz-mid in Wang et.al 2016. This material has been characterized by Wang et.al. (2016) by EXAFS; they report it consists for approximately 35% of becquerelite and 40% of metaschoepite ($UO_3(H_2O)_2$) and suggest that becquerelite ($Ca(UO_2)_6O_4(OH)_6{\cdot}8(H_2O)$) forms from metaschoepite in the presence of calcium from the soil. This fraction was selected because the uranium content is considerably higher than in the outer fraction, which contains more impurities from the soil. SEM analysis showed micrometer scale aggregates made up of sub-micrometer scale particles (Wang et.al , 2016) Visually, aggregate sizes varied considerable; the DUCP-Hz-mid fraction was heterogeneous in particle size. The elemental composition comprised 54% U, 3 % Ca, 1% Mg, 1% Si, 3% other metals and 38% other metals.

For regulating the experimental pH, the non-metal-complexing tertiary amine (“Better”) buffers PIPPS (1,4-piperazinedipropanesulfonic-acid, at pH=3.0 and 4.5), MES (2-(*N*-morpholino)ethanesulfonic-acid, at pH=6.0) and MOPS (3-(*N*-morpholino)propanesulfonic-acid, at pH=7.5) and DEPP (N, N’-diethylpiperazine, at pH 9) were used. Oxalic acid (Merck; pro analysis), and sodium humate (Sigma Aldrich; technical grade) were used as uranium complexing ligands. CO_2 gas with a purity of 4.5 was used for increasing the CO_2 partial pressure. Additionally, NaCl (Merck; pro analysis), NaOH (Amresco; reagent grade) and nitric

acid (Fisher; trace metal pure) were used. Experimental solutions were prepared with ultrapure water (UPW)

2.2 Methods

2.2.1 BET measurement

The specific surface area of the DU corrosion product was measured with the BET-N_2 method. The BET set up is a method to generate the specific surface area of a solid by the adsorption of gas molecules by the characterized material. There the gas molecules are attracted to the surface by dispersion forces. The spezific surface area is than calculated using the adsorbed gas volume. The more gas volume is adsorbed the higher is the spezific surface area (Heister, 2014).

For the BET-N_2 run, a certain amount of the depleted uranium corrosion product was weighed in (0.208g). The material was poured in to a viole and closed air-tight . The viole was connected into the BET-construction and the material was heated over one night in order to dehydrate the material. The measurement resulted in a specific surface area of 9.7m^2/g.

The specific surface area was used for the calculation of the dissolution rate. The dissolution rate was normalized by the specific surface area, in order to generate values comparable to previous studies.

2.2.2 Dissolution Experiments

2.2.2.1 Batch experiments

Two types of dissolution experiments were carried out: batch experiments and continuous flow stirred tank reactor (CFSTR) experiments. The aim of the batch experiments was to establish how the risk of uranium dissolution from DU penetrators in the soil relates to specific environmental parameters. In this context we have examined the following parameters: pH, ionic strength, suspension density, CO_2 partial pressure and the presence of ligands.

The CFSTR experiments were carried out to examine the effect of solution saturation state for the minerals present in the DU corrosion product on the dissolution rate. Contrary to the batch experiments in the flow-through experiments the degree to which dissolution reaction products accumulate in solution can be controlled by regulating the flow rate.

The general procedure (batch)

DU corrosion product dissolution experiments were carried out in polyethylene containers (except for pCO_2=0 experiment; glass containers were used) at 20 (±1) °C. Experimental solution including electrolyte, pH buffer and if applicable other chemicals were prepared and pre-equilibrated with the atmosphere by pumping through air for 3 days prior to addition of the DU corrosion product. Two exceptions to this were the p CO_2 = 0 experiment, wherein the experiments were started once the pH had stabilized, and the CO_2-free experiment, wherein water for solutions was boiled and N_2-gas was bubbled through in order to prevent air re-intake. After introduction into the anaerobic chamber, the solutions were prepared and left for three days in order to ensure N_2-atmosphere only. The default suspension density was 100 mg l^{-1} corrosion product, the default pCO_2 was 3.5 (atmospheric), the default pH-buffer concentration was 5 mM and the default electrolyte concentration was 10 mM NaCl. Samples were taken after 0.25, 0.5, 1, 2, 4, 8, 24, 48, 96 and 192 hours and filtered over 0.1 µm PVDF syringe filters (Millex). Sub-samples were acidified with nitric acid and U concentrations determined by ICP-MS. Experiments were carried out in duplicates.

Figure 1: The picture shows the filtering of the suspension through the syringe filter (0.1µm Millex) (Source:Sebastian Pontz)

pH

The effect of pH on the dissolution rate was examined for 5 pH values within the soil-relevant pH-range (3-9): 3, 4.5 6, 7.5 and 9. The pH was maintained a the set pH by a suitable pH buffer and remained constant throughout the experiment (± 0.3 pH units).

Ionic-strength

The effect of ionic strength on the dissolution rate was examined by varying the NaCl concentration: 10, 30 and 100 mM NaCl. Experiments were done at pH 7.5, because dissolution within the timespan of the experiments remained remote from complete dissolution of the DU corrosion product.

Suspension-density

The effect of suspension density on dissolution rate was examined by varying the suspension density: 10, 30 and 100 mg L^{-1} at pH 7.5. By these experiments it was verified if dissolution rate scaled with surface area of the DU corrosion product.

CO_2-partial-pressure

The effect of formation of soluble uranyl carbonate complexes on the dissolution rate was

examined by varying the CO_2 partial pressure: no CO_2, and a pCO_2 of 0 and 3.5, at pH 7.5 and 9. Only these two pH values were included, because below pH 6 equilibrium concentrations of carbonate and bicarbonate are low compared to carbonic acid and were assumed to have little effect on dissolution. The no CO_2- experiment was carried out in a Coy-tent (Vinyl anaerobic chamber, COY) under a N_2 atmosphere (Formiergas 95/5, Linde); water used for preparing solutions was pre-boiled.

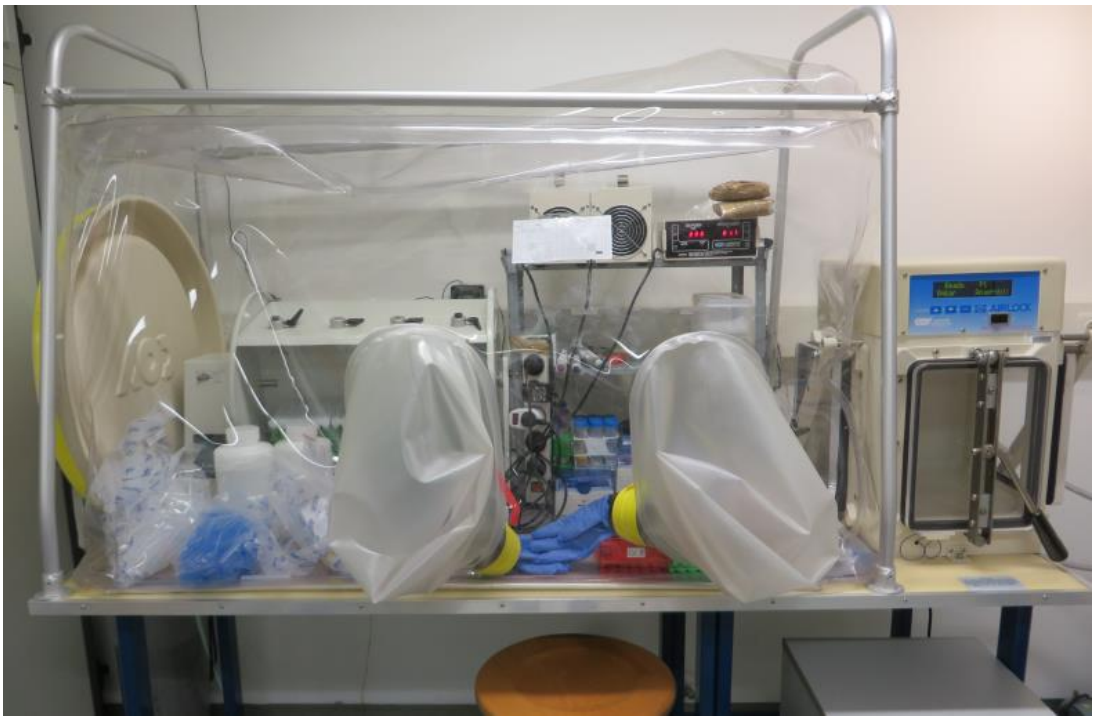

Figure 2: This picture shows the COY-tent, where the experiment without CO2 had taken place (Source:S.P.)

A solution in equilibrium with pCO_2 = 0 was prepared by continuously bubbling CO_2 gas through a buffered solution and adjusting the pH with NaOH solution; the experiment was started once the pH had become stable at the desired value. The solutions were then poured into a glass bottle that was closed with a septum to prevent gas exchange with the environment. Samples were taken with a syringe with a needle.

Figure 3: The picture shows the pCO_2=0 treatments (Source:S.P.)

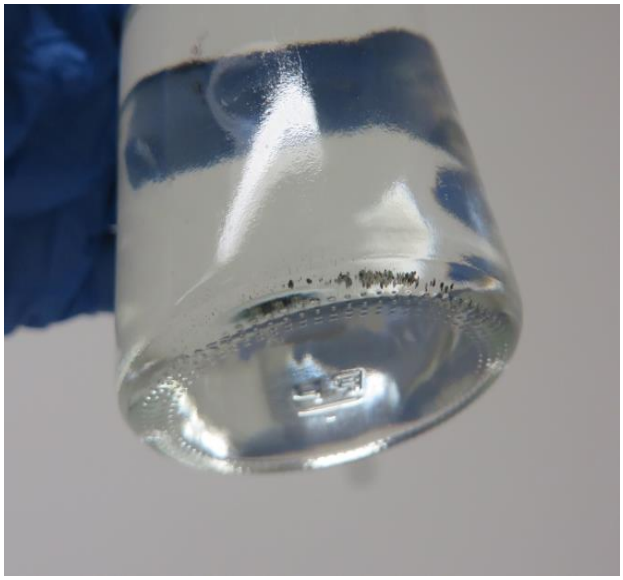

Figure 4:DU particles settled on the bottom of the flask

Presence of ligands

The effect of two naturally occurring ligands on the dissolution rate was examined for 1 mM oxalate at pH 4.5, and for 66 mg l^{-1} humate at pH 4.5 and 6. The humate concentration corresponds with a 2 mM C (carbon) concentration, equal to the carbon concentration in the oxalate treatment.

Figure 5 and Figure 6: Treatment with humic acid, in figure 6 DU particles are visible (Source:S.P.)

The dissolution rates were calculated by linear regression of the uranium concentration data as a function of time, for the linear section of the dissolution curve, comprising a minimum of four data points. The slope of the regression line was divided by the specific surface area of the DU corrosion product.

In order to compare the results derived from the lab-work, geochemical calculations has been done using the computer program PHREEQC version 3.

2.2.2.2. CFSTR experiments

The polymethylmethacrylate reactor with an inner volume of 96 ml was placed on a stirring plate and was stirred by means of an incorporated magnetic stirring bar at 20 (±1) °C. DU corrosion product was added through a port on the top of the reactor to a suspension density of 0.1 g l^{-1}. The influent solution consisted of 10 mM NaCl and 5 mM MOPS (pH 7.5). The inflow rate was regulated by means of a peristaltic pump (Gilson). The effluent solution was filtered over a 0.025 µm filter (cellulose nitrate membrane filter, Schleicher and Schuell), that was mounted on top of the outlet at the bottom of the reactor.
Prior to sampling, the reactor first equilibrated for 8 days to reach an approximate initial steady state. The flow rate was varied stepwise: 0.6, 0.15, 0.1, 0.05, 0.02 ml min^{-1}. For each flow rate, samples were taken over time until an approximate steady state U concentration in the effluent had been reached and at least 3 reactor volumes had been pumped through (corresponding with ≈ 95% of the final concentration). Samples were acidified with nitric acid and U concentrations were determined by ICP-MS.

Dissolution rates were calculated from the effluent concentration (C_{eff}) data by averaging the concentration for the last four time points at a given flow rate and dividing the concentration by the residence time (t_{Res}), suspension density (SSR) and specific surface area (SSA) of the corrosion product (rate= $C_{eff}/(t_{Res}*SSA*SSR)$)

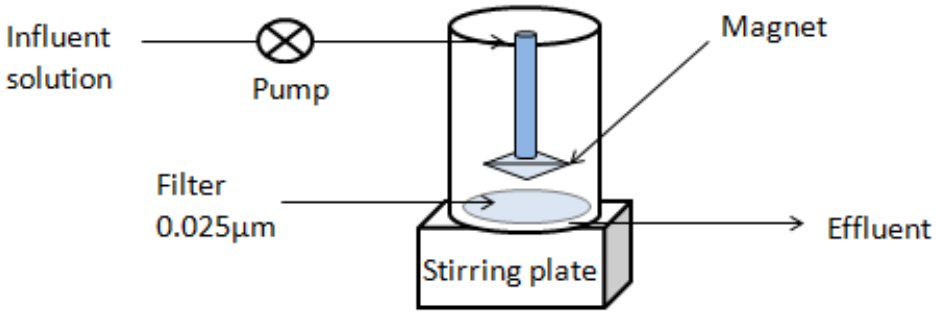

Figure 7: Schematic representation of the CFSTR set up

3 Results and Discussion-Dissolution of DU corrosion products

3.1 Batch experiments

The mineralogy of DU corrosion products has been investigated in this study by the group of Prof. Bernier Latmani at EPFL. The corrosion products contain various U(VI) bearing minerals that each have different thermodynamic properties and reactivities. The solubilities of such phases has been reviewed previously, e.g. by Gorman-Lewis et al (2008) , and thermodynamic data are found in various carefully compiled databases (Guillaumont, 2003) (Gorman-Lewis, 2008). The dissolution rates of U(VI) bearing minerals has also been investigated by a number of researchers (Pérez I. I., 1996, S. Steward, 1996, Pérez I. I., 2000, Giammar, 2002, Reinoso-Maset, 2017, Wang G. W.-M., 2017). However, relating the dissolution of heterogeneous DU corrosion products to pure phase dissolution rate data may not be straightforward due to the heterogeneous mixture of minerals in the corrosion products and due to the environmental variables and reaction times that influence the composition of these products. The release from DU corrosion products coupled to transport in a sand column was observed in column experiments by Handley Sidhu et al (2009). Liu et al. (2004) studied the dissolution rates of uranyl silicate microprecipitates in sediments at

the Hanford site. In this study the dissolution rates of DU corrosion products in batch and continuous flow stirred tank reactor (CFSTR) setups were studied. We have investigated geochemical parameters which are likely to influence dissolution behaviour, including pH, pCO_2, ionic strength (salinity), suspension concentrations, and the presence and absence of organic ligands including humic acids.

The suspension density in batch reactors of 100 mg/L corresponds to a total Uranium concentration of approximately 225 µM uranium according to the observations of the group of Prof. Bernier-Latmani in the same project (54 % uranium by mass in the DU corrosion product). In some experiments total uranium concentrations exceeded this concentration slightly, suggesting some inhomogeneity in the DU corrosion product.

3.1.1 Effect of pCO2

The effect of pCO2 on the dissolution of DU corrosion products has been tested in batch experiments at pH 7.5 and pH 9. The summarized results are shown in Figure 8 and Figure 9.

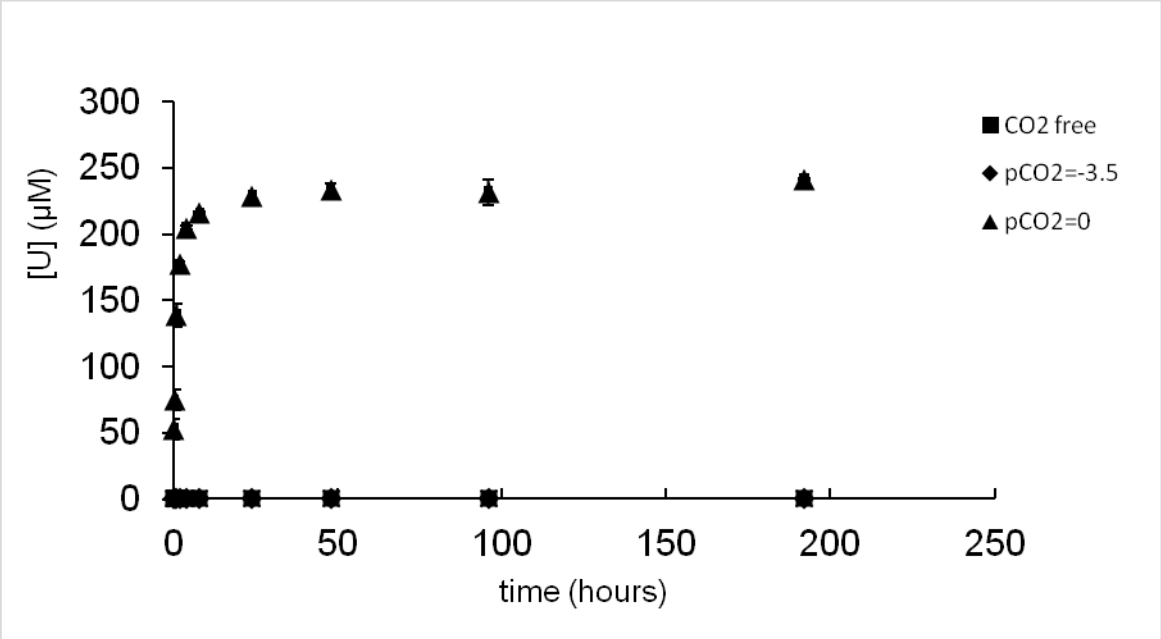

Figure 8. Effect of pCO2 on uranium dissolution at pH 7.5 (5mM MOPS). Susp. density: 100 mg/L; I =0.01M (NaCl).

The increase in pCO_2 from CO_2-free conditions via atmospheric pCO_2 to a pure CO_2 atmosphere affords strongly increasing solubilites and dissolution rates. It is not possible to derive uranium solubilities in equilibrium with the DU corrosion product from these data. In dissolution experiments in equilibrium with a pure CO_2 atmosphere, uranium in DU corrosion products dissolved completely. At lower pCO_2 steady state concentrations due to solubility equilibrium was observed in some cases. At pH 7.5, the steady state concentrations of soluble uranium reached approximately 0.8 and 0.08 µM in the presence of atmospheric CO_2 or in CO_2 free system, respectively (Figure 8). This is consistent with calculated soluble uranium concentrations in equilibrium with metaschoepite (1.1 and 0.08 µM) using the solubility constant of Meinrath et al (1996) (1.1 and 0.08 µM) but somewhat lower than predictions based on the Metaschoepite solubilities reported by Giammar et al. (2004)) (3.6 and 1 µM) (Meinrath, 1996, Giammar and Hering 2004). Given the variability of reported solubility coefficients, it shows that the solubility of DU corrosion products seem to be approximately consistent with metaschoepite solubilities, despite the heterogeneous nature of the corrosion products. At pH 9 (Figure 9) steady state uranium concentrations are only reached in the absence of CO_2 within the timeframe of the experiments at approximately 0.3 µM, corresponding to calculated solubilities of metaschoepite of 0.3 µM using the solubility constant of Meinrath et al (1996). The depletion of solid phase uranium in the batch experiments due to dissolution, particularly in pure CO_2 atmosphere, lead to non-linear dissolution rates at dissolved concentrations above 100 µM. Therefore, initial net dissolution rates from batch experiments as discussed in the sections below were calculated from the slopes of the linear section of the dissolution versus time graphs and no data points with soluble uranium concentrations above 100 µM were used. The observed DU corrosion product dissolution rates ranged from 0.012 µmol m^{-2} h^{-1} at pH 7.5 and atmospheric CO_2 to 73.02 µmol m^{-2} h^{-1} at pH 7.5 in a pure CO_2 atmosphere. Steward and Mones (1996) observed a dissolution rate for dehydrated schoepite at pH 9 of 0.02 µmol m^{-2} h^{-1} at a pCO_2 of -4 and >0.26 µmol m^{-2} h^{-1} at a pCO_2 of -3 while we observed dissolution rates of 0.33 µmol m^{-2} h^{-1} at pH 9 and a pCO_2 of -3.5 (Steward and Mones 1996). Considering the heterogeneous mineralogy of DU corrosion product and the potential differences in reactive surface area, the match between these published values and our results can be seen as rather consistent. At pH 7.5, the dissolution rates are not significantly influenced by atmospheric CO_2 as

compared to CO_2–free conditions. In a pure CO_2 atmosphere, dissolution rates increase by more than an order of magnitude (Table 1). At pH 9, atmospheric pCO_2 leads to a 6.5-fold increase of dissolution rates compared to CO_2–free conditions and in a pure CO_2 atmosphere, dissolution rates again increase by an order of magnitude.

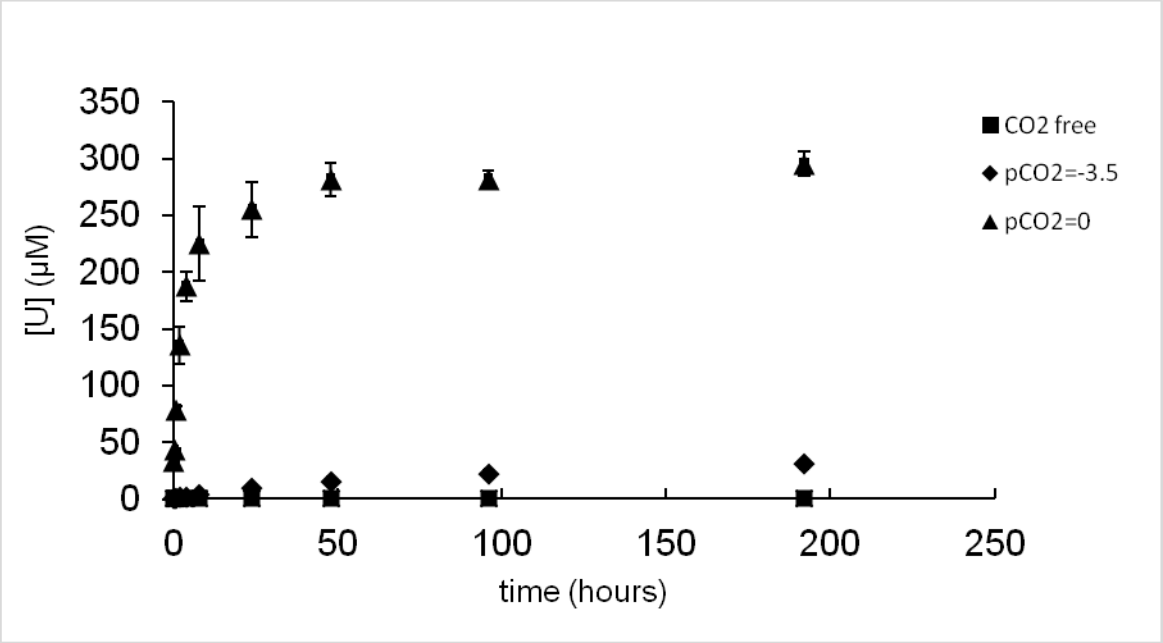

Figure 9. Effect of pCO2 on uranium dissolution at pH 9 (5mM DEPP). Susp. density: 100 mg/L (=225 µM U/L); I =0.01M (NaCl).

Treatment type	Dissolution rate (µmol m^{-2} h^{-1})
No CO_2; pH 7.5	0.019
pCO_2=-3.5; pH 7.5	0.012
pCO_2=0; pH 7.5	73.02
No CO_2; pH 9	0.050
pCO_2=-3.5; pH 9	0.33
pCO_2=0; pH 9	42.90

Table 1. Effect of CO2 on DU corrosion product dissolution rates. Susp. density: 100 mg/L (=225 µM U/L); I =0.01M (NaCl)

The significant effect of carbonate on U(VI) solution speciation and on the solubility and the dissolution rates of U(VI) from uranium bearing minerals is well known. The availability of thermodynamic data on the stability of soluble carbonate and calcium-carbonate complexes together with solubility constants of relevant minerals allows the prediction of the CO_2 effect on solution speciation and solubility (Gorman-Lewis, Burns et al. 2008). The effect of carbonate on dissolution rates has also been investigated for pure of phases (Pérez, Casas et al. 1996, De Pablo 1999, Pérez, Casas et al. 2000, Sowder 2001, Ilton 2006, Gudavalli 2013, Reinoso-Maset, Steefel et al. 2017). For example, Reinoso-Maset et al. (2017) found 2 to 3 orders of magnitude higher dissolution rates of uranium oxyhydroxides as the dissolved carbonate concentration increases by one order of magnitude. With a pH increase from 7.5 to 9 in equilibrium with atmospheric pCO_2, the total dissolved inorganic carbon increases by approximately 1 order of magnitude. The corresponding acceleration of dissolution rates by a factor 30 may be largely triggered by a CO_2 promoted dissolution mechanism. However, it should be noted that the dissolution rates also increased in the absence of CO_2 by a factor 2.5, suggesting that a smaller effect of an alkaline dissolution mechanism also influenced dissolution rates in this pH range. At constant pH 7.5, an increase of pCO2 from ambient conditions to a pure CO_2 atmosphere leads to an increase of total dissolved inorganic carbon of about 3.6 orders of magnitude lead to an increase of net dissolution rates by a 3.8 orders of magnitude.

3.1.2 Effect of solution pH on dissolution rates

While we have already explored the dissolution of DU corrosion products at neutral to high pH, we also investigated dissolution in the acidic pH range between pH 3 and 6 in equilibrium with ambient air (Table 2, Figure 10).

pH	Buffer	dissolution rate [µmol m-2 h-1]
3	PIPPS	40.37
4.5	PIPPS	1.90
6	MES	0.0073
7.5	MOPS	0.012
9	DEPP	0.33

Table 2. Observed initial dissolution rates as a function of pH. Suspension densities in the batch reactors were 100 mg/L and the solution contained 5 mM pH-Buffer and 10 mM NaCL.

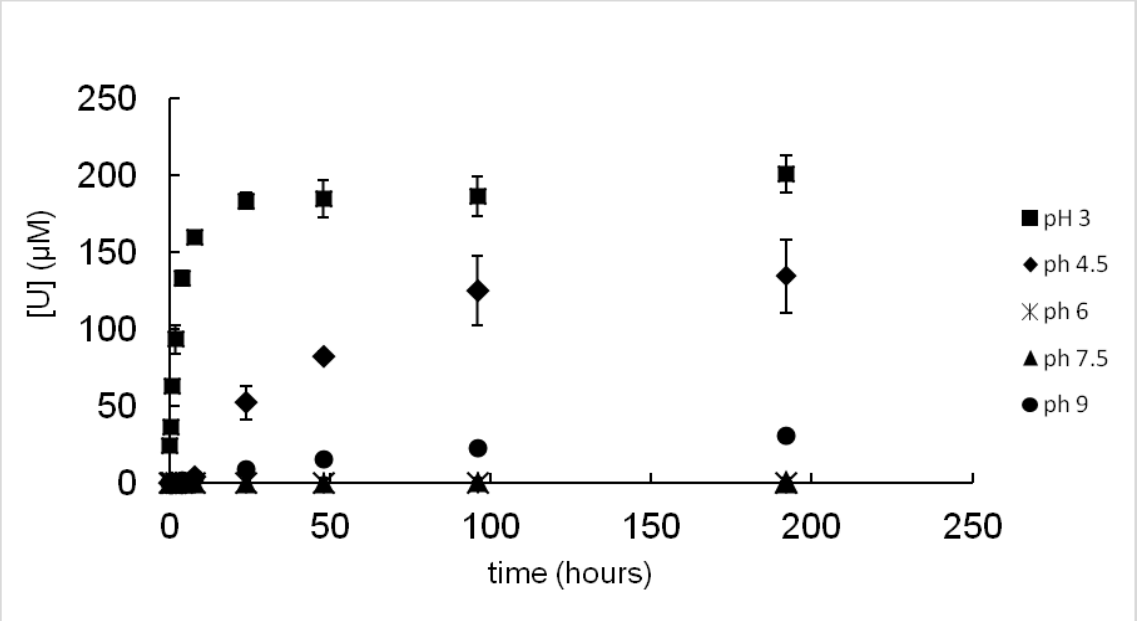

Figure 10: Dissolution of DU corrosion products at pH 3 to 9. Close to total dissolution of uranium from DU corrosion products is observed at pH 3. Ambient pCO2; Susp. density: 100 mg/L (=225 µM U/L); I =0.01M (NaCl).

Given the limited time of the dissolution experiments, steady state soluble uranium concentrations were not reached at all pH values (Figure 10). Even if steady state concentrations are reached, we cannot unambiguously relate these concentrations to equilibrium solubility of a mineral phase as it may reflect steady state rates of mineral transformation reactions. However, in order to compare our results to equilibrium solubility calculations based on the solubility of metaschoepite (using the solubility constant of Meinrath et al (1996)) we have plotted the uranium concentrations after 200 h reaction time as a function of pH along with the calculated metaschoepite solubility (Figure 11) (Meinrath, Kato et al. 1996). In general, we see reasonable consistency between calculated and observed uranium concentrations.

Initial net dissolution rates varied strongly with pH. At pH 3 maximum net rates were observed. In the acidic pH range carbonate promoted dissolution plays only a minor role due to the low carbonate solubility in equilibrium with ambient air. The dominant dissolution mechanism here is presumably a proton promoted dissolution mechanism that is well known for many metal oxides (Wieland, 1988). Similarly, the dissolution of UO2 has been found to be accelerated by a proton-promoted detachment of U(VI) from the mineral surface (Ulrich, 2008). At increasing pH the net dissolution rates decrease until a minimum rate is observed at pH 6. As discussed in the previous section, dissolution rates increase with further increasing pH, mainly due to increasing soluble carbonate concentrations and to a minor extend due to an alkaline dissolution mechanism. The non-carbonate dependent dissolution rates are consistent with studies demonstrating that the molecular-scale rate-determining step in this case is the detachment of uranyl from the surface which is accelerated by bonding of hydroxyl groups or H+ to surface oxygen sites that weaken the corresponding U-O-U bonds (Schindler, 2004).

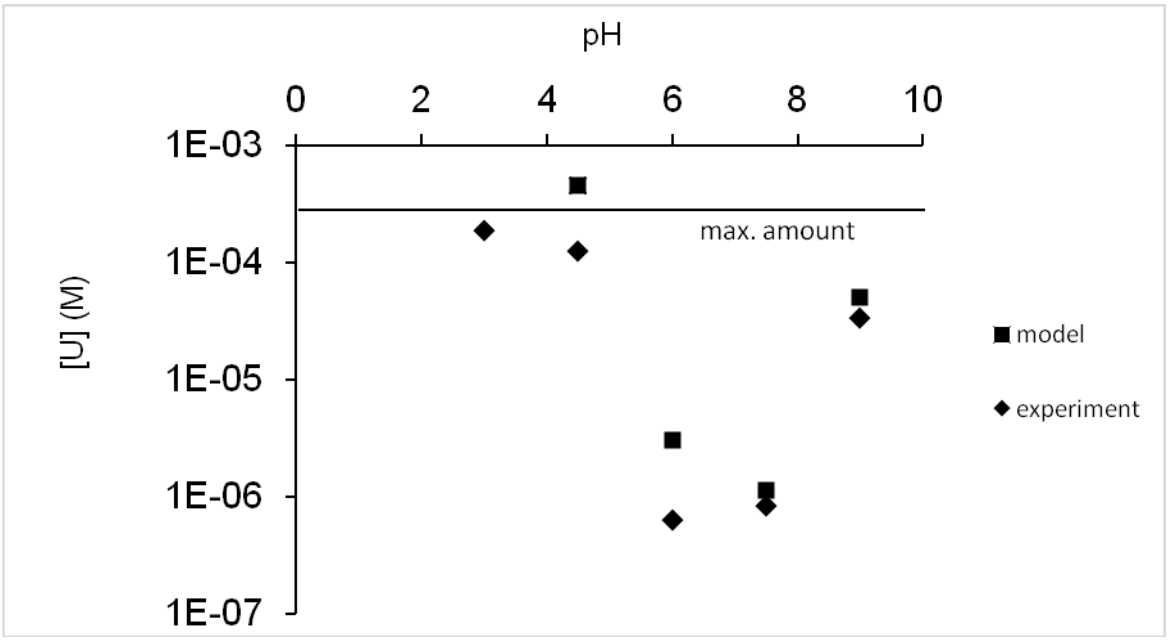

Figure 11. Maximum soluble uranium concentrations observed in batch dissolution experiments as a function of pH and modelled solubilities of metaschoepite. The total concentration of uranium added as DU corrosion product is 225 µM (solid line). Ambient pCO2; Susp. density: 100 mg/L (=225 µM U/L); I =0.01M (NaCl).

3.1.3 Effect of NaCl concentrations on dissolution rates

The effect of ionic strength on mineral dissolution is often studied by increasing additions of a salt such as NaCl. The underlying assumption is that the changing electrolyte concentrations influences the activity of charged soluble species and the structure of the electrostatic field above charged mineral surfaces, but that all other specific chemical interactions between the electrolyte components and the mineral or soluble species are negligible. As we have seen earlier, carbonate would not qualify as electrolyte in this sense. However, various U(VI) oxohydroxides including the main mineralogical components of DU-corrosion products have a layered structure incorporating a variety of cations and/or water molecules in the interlayer space and are connected by hydrogen bonds.

For example, among the main components of DU corrosion product becquerelite has calcium in the interlayer space, while metaschoepite and studtite have no interlayer cations (Burns, 2002). Reinoso-Maset et al. (2017) investigated the solution behaviour of U(VI) oxohydroxides containing interlayer cations and found that cation exchange had only a minor effect on their dissolution. This is consistent with the detachment of U(VI) from the surface constituting the rate-determining step in the dissolution mechanism as discussed above.

We investigated the effect of NaCl concentrations on the dissolution of DU corrosion products as shown in Table 3 and Figure 12. In the presence of 30 and 100 mM NaCl, steady state uranium concentrations were not reached in the timeframe of the experiments. In order to allow for a qualitative comparison between calculated uranium solubilities of metaschoepite (using the solubility constant of Meinrath et al (1996)) with our observations, we plotted the modelled concentrations along with the uranium concentration at the end of the dissolution experiment (which corresponded to the maximum observed uranium concentrations) as a function of NaCl concentrations in Figure 13 (Meinrath, Kato et al. 1996). The predicted increase of metaschoepite solubility with electrolyte concentrations were consistent with increasing dissolved concentrations of uranium in the presence of DU corrosion products. As the model does not include the possible effect of cation exchange in the uranyl oxohydroxide structures on their solubilities, the ionic strength effect seems to be related to shifts in activity coefficients of uranyl- and carbonate species.

NaCl [mM]	Max. uranium conc. [µmol L-1]	Init. net diss. rate [µmol m-2 h-1]
10	1.1	0.012
30	1.6	0.1
100	2.2	0.12

Table 3. Observed maximum dissolved U(VI) concentrations and initial dissolution rates as a function of NaCl concentrations. Suspension densities in the batch reactors were 100 mg/L, solution pH 7.5 (5 mM MOPS) and variable concentrations of NaCl.

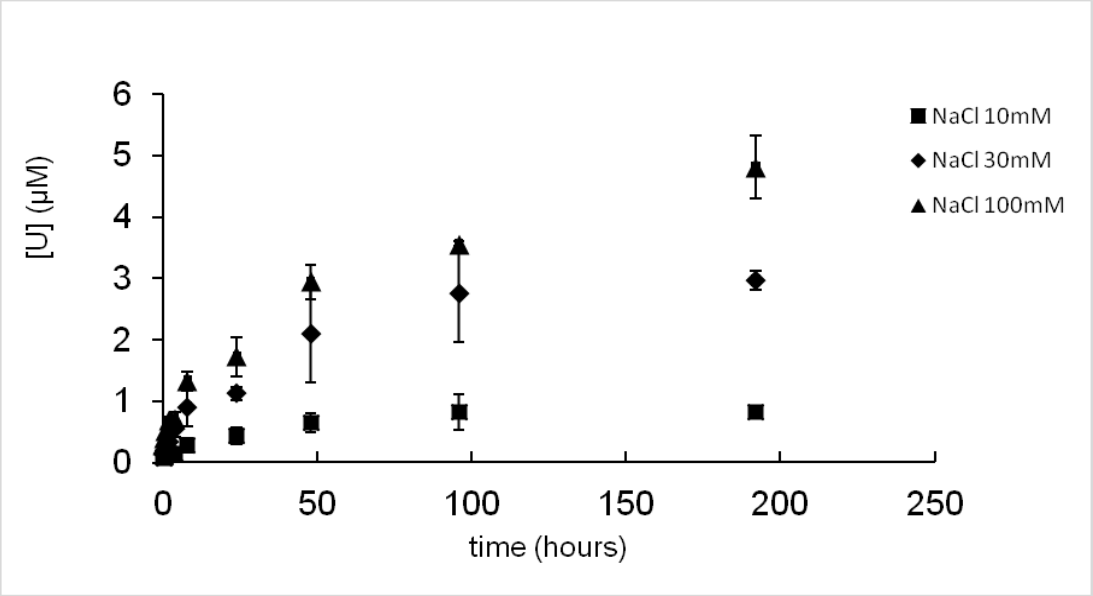

Figure 12. Dissolution of uranium at different ionic strength at pH 7.5 (5mM MOPS). Ambient pCO2; Susp. density: 100 mg/L.

The effect of NaCl concentrations on dissolution rates were significant. An order of magnitude increase of NaCl concentrations lead to an order of magnitude increase in net initial dissolution rates (Table

Similar accelerating effects of increasing ionic strength on uranyl oxohydroxyde dissolution rates have been reported previously (Roelofs, 2007). As linear dissolution rates are expected far from equilibrium, we do not expect that the change of solubilities as a result of ionic strength variations should affect the kinetics of uranium dissolution. However, ionic strength changes can have a clear effect on the electrostatics of the mineral surface and, therefore, on the surface speciation. As discussed above, the rates of both the carbonate promoted dissolution as well as the proton promoted- and alkaline dissolution depend on the formation of surface species that are precursors to the rate-determining dissolution step and may therefore be influenced by adsorption processes.

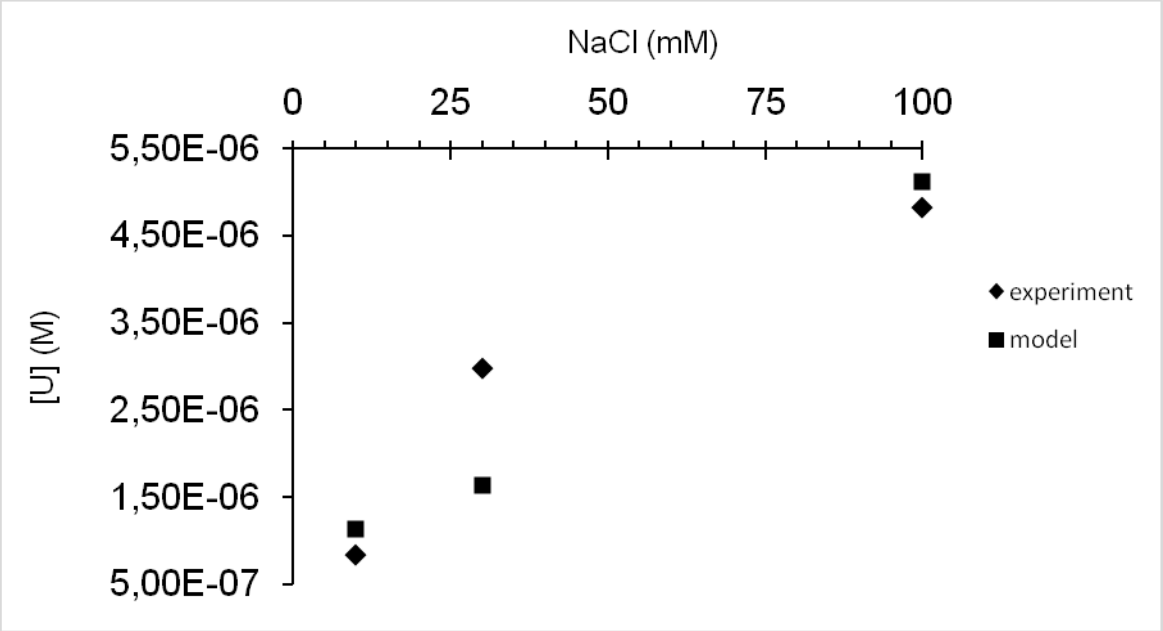

Figure 13. Effect of ionic strength (NaOH) on metaschoepite solubility calculated by thermodynamic equilibrium modelling in comparison to maximum uranium concentrations in DU corrosion product dissolution experiments. pH 7.5; ambient pCO2; Susp. density: 100 mg/L.

3.1.4 Effect of Suspension density on the dissolution of DU

In order to see how the solid solution ratio affects the dissolution experiments with different suspension densities has been carried out (Figure 14). The solutions has been brought to pH 7.5 by using the buffer MOPS (5mM).

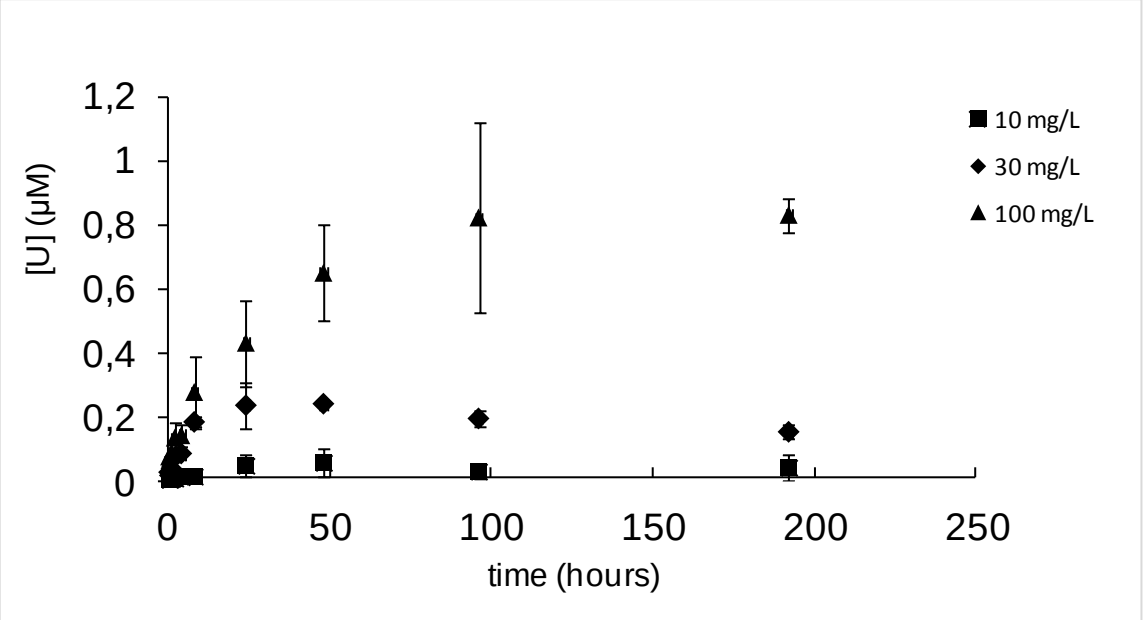

Figure 14: Comparison of suspension-density effect on the dissolution of DU, c(NaCl)=10mM. Varying suspension densities: 10mg/L and 30mg/L

At a suspension density of 10mg/L the uranium dissolves slowly in the first 8 hours. After the initial stage, dissolution of uranium went up, resulting in a concentration peak at 48 h. Thereafter it decreases within the next two days and rises again to the end. After 196 h a concentration of about 0.05 µM is reached. At 30 mg/L suspension density the concentration increases within the first 24 hours, where it stagnates and falls down continuously for the last 172 hours.

The dissolution of uranium oxides seems somehow to be influenced by the solid/solution ratio meaning the amount of solid in relation to the solution volume. The dissolution

decreases with decreasing amount of uranium oxide. Equilibrium is in not reached in these treatments (10mg/L, 30mg/L).

These findings only prove the variety of the DU corrosion product. The material is composed of three uranium oxyhydroxides . Wang et. al. (2016) identified those different phases as Metaschoepite, Bequerelite and Studtite. The solubility of metaschoepite is found to be lg K_{sp}=4.68 to 6.23. Bequerelite for instance is much less soluble with lg Ksp=41.89 to 43.70. At higher suspension density, the amount of a phase, which is more soluble is increased (metaschoepite), thus the concentration of dissolved uranium also increases.

3.1.5 Effect of organic ligands on the dissolution of DU corrosion products

Dissolution rates of oxide minerals can be significantly increased by adsorbed organic ligands in a ligand-controlled dissolution mechanism (Furrer and Stumm 1986). The adsorbed ligands kinetically labilize surface sites and the detachment of the sites is considered to be rate determining. In order to investigate such effects of an organic ligand, we studied the effect of oxalic acid on the dissolution of DU corrosion products. Oxalate is produced by fungi and is formed in many plant species and is known to form stable uranyl complexes in solution (Vallet, 2003; Crea, 2007). Oxalate can also be seen as a model for uranium complexation by fulvic acids. We investigated the effect of oxalate on DU corrosion product dissolution at pH 4.5 in order to understand the effect of such compounds in acidic soils such as podsols. The results of dissolution experiments including rate coefficients and maximum soluble U(VI) concentrations are shown in Figure 15 and Table 4. Uranium concentrations were higher in the presence of oxalate compared to solutions in the absence of the organic ligand. In the presence of oxalate, almost all uranium contained in the DU corrosion product was found in solution, therefore, the data contain no indication of equilibrium solubilities. However, the modelled U(VI) solubility using uranium oxalate stability constants of Crea et al. (2007) and metaschoepite solubility constant of Meinrath et al (1996) increased from 4.6 10^{-4} M to 1.4 10^{-3} M U(VI) in the absence and presence of 1 mM oxalate (Meinrath, Kato et al. 1996, Crea, De Robertis et al. 2007).

oxalate [mM]	Init. net diss. rate [µmol m-2 h-1]
0	1.90
1	24.78

Table 4. Observed initial dissolution rates of DU corrosion products in the presence of 1 mM oxalate and in the absence of oxalate. Ambient pCO_2; Susp. density: 100 mg/L (=225 µM U/L); I =0.01M (NaCl); pH 4.5 (5 mM PIPPS).

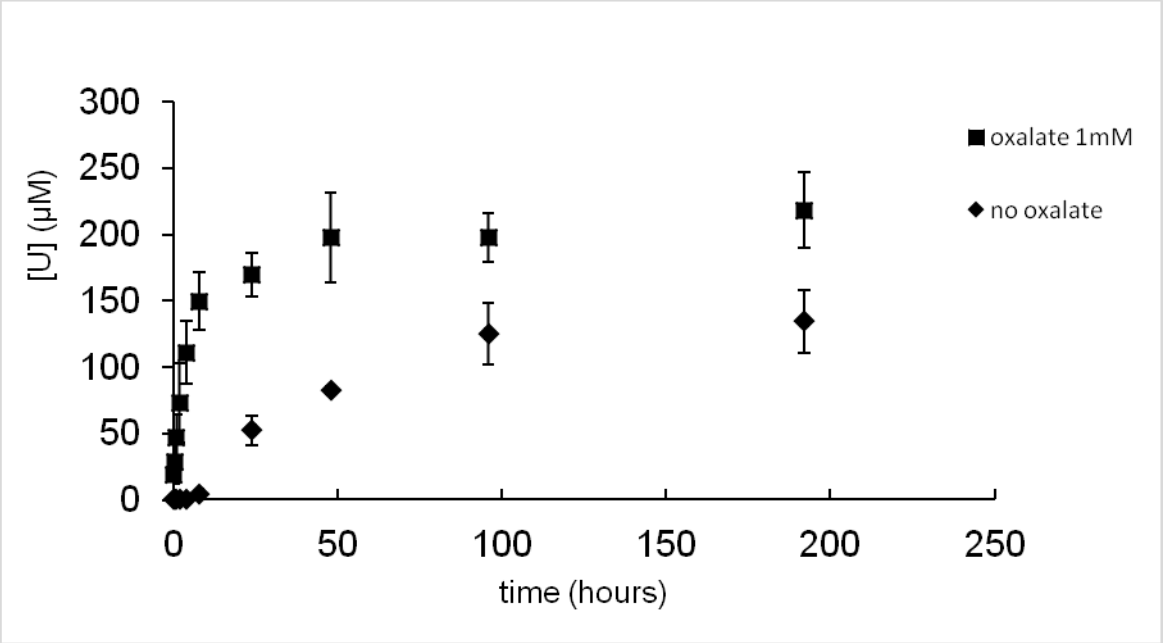

Figure 15. Dissolution of DU corrosion products at pH 4.5 (5mM PIPPS) in the presence and absence of 1 mM oxalate. Ambient pCO2; pH 4.5; Susp. density: 100 mg/L; I =0.01M (NaCl).

The initial net dissolution rates increased by more than an order of magnitude in the presence of 1 mM oxalate compared to the oxalate free experiment. For a more detailed investigation of the dissolution mechanism, more work is needed. However, these data

indicate an accelerating role of ligand controlled processes for DU corrosion product dissolution.

3.1.6 Effect of humic substance on dissolution rates

Natural organic matter (NOM) has a high affinity for binding uranyl as soluble complexes or organic colloids (Degueldre 2014; Bone 2017; Dublet 2017). Humic acids (HA) and their metal complexes also strongly sorb to metal oxide surfaces (Vermeer, 1998). HA are polymers with numerous functional groups that may simultaneously interact with several surface sites of a metal oxide by specific bonding. However, the formation of multinuclear surface complexes tends to inhibit dissolution (Biber, 1994). Inhibition of metal oxide net dissolution by NOM at acidic pH has been observed previously and was attributed to protection of the surface by adsorbed HA as well as adsorption of the dissolving metal ions by the adsorbed HA (Yoon, 2005).

In order to investigate the effect of HA on DU corrosion product dissolution, we performed batch dissolution experiments at pH 4.5 and 6 in the absence and presence of 66 mg/L HA (Table 5 and Figure 16).

Steady state uranium concentrations were not reached in any of the experiments. Therefore, maximum observed uranium concentrations during the experiments are controlled by dissolution rates. However, these rates decline over the progress of reaction time in most dissolution experiments indicating that steady state conditions are approached. Maximum observed uranium concentrations at pH 4.5 are significantly lower in the presence of HA compared to maximum concentrations in its absence. Also, net initial dissolution rates are lower in the presence of HA. This inhibitory effect is contrasted by a dissolution promoting effect of HA at pH 6 leading to higher maximum uranium concentrations and accelerated dissolution rates. Various effects may contribute to these observations including pH dependent adsorption of HA, co-adsorption of uranium with HA, protection of surface sites by adsorbed HA, binding of uranium by dissolved or colloidal HA and coagulation of HA as a function of pH and adsorbed uranium concentrations. Clearly, the results reported here are insufficient for elucidating the relative role of all these processes. However, it becomes clear that HA has a complex pH effect on dissolution of DU corrosion products. As the organic

substance content of soils and aquifer materials can vary widely, this effect needs further investigation

Humic substance [mg/L]	pH	Max. uranium conc. [µmol L-1]	Init. net diss. rate [µmol m-2 h-1]
0	4.5	134.6	1.9
66	4.5	38.4	1.32
0	6	0.66	0.0073
66	6	17.3	0.77

Table 5. Observed initial dissolution rates of DU corrosion products in the presence of 66 mg/L humic substance and in its absence at pH 4.5 (5 mM PIPPS) and pH 6 (5 mM MES). Ambient pCO_2; Susp. density: 100 mg/L (=225 µM U/L); I =0.01M (NaCl).

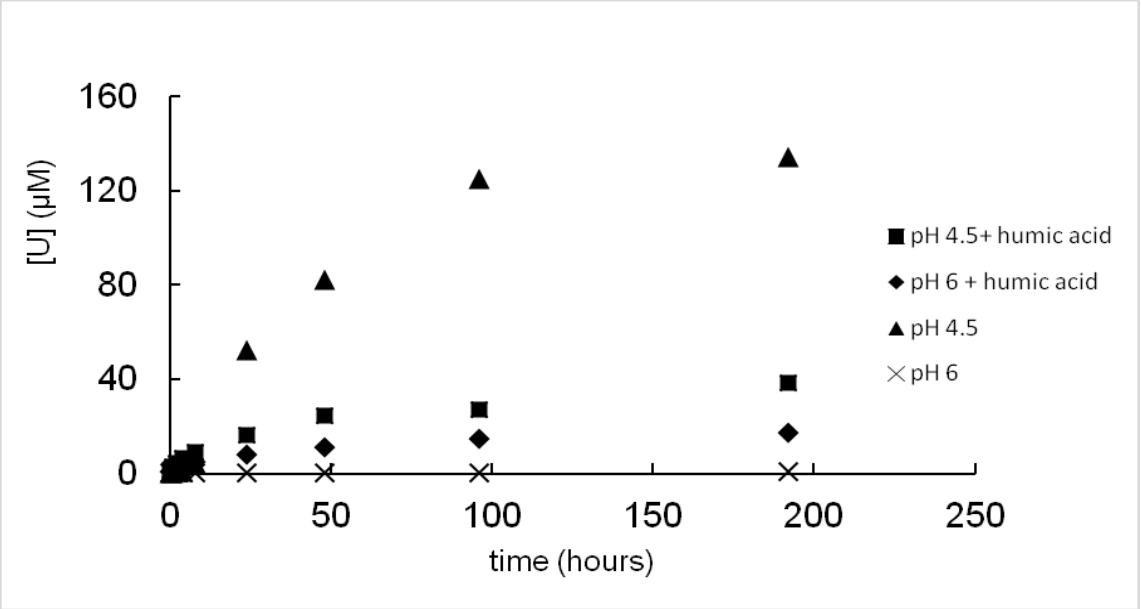

Figure 16. Dissolution behavior of DU in the absence and presence of humic acid at pH 4.5 (5mM PIPPS) and 6 (5mM MES). Ambient pCO2; humic substance conc.: 66 mg/L; Susp. density: 100 mg/L; I =0.01M (NaCl).

3.2 Dissolution of DU in Continuous Flow Stirred Tank Reactor (CFSTR)

The advantage of continuous flow reactors over batch dissolution setups is that reaction products are continually removed from the reactor. This allows to remove possible labile species and to observe quasi steady state dissolution conditions (Kraemer and Hering 1997). It should be noted that the solids in the reactor keep dissolving and that this can impair steady state observations. However, for this investigation, we chose a pH of 7.5 where dissolution rates are low and only a few percent of the total uranium in the reactor dissolved over the timescales of the experiments. Figure 17 shows an example for steady state setting in after increasing a flow rate (6 hours after the start of the reactor run). The average of the last four data points shown in the graph were used to calculate dissolution rates under these conditions.

The goal of the CFSTR dissolution experiments was to verify that a) initial dissolution rates from batch experiments are a reasonable approximation of steady state dissolution rates and b) to investigate the effect of the solution saturation state and Gibbs free energy of reaction ΔG influence the observed dissolution rates.

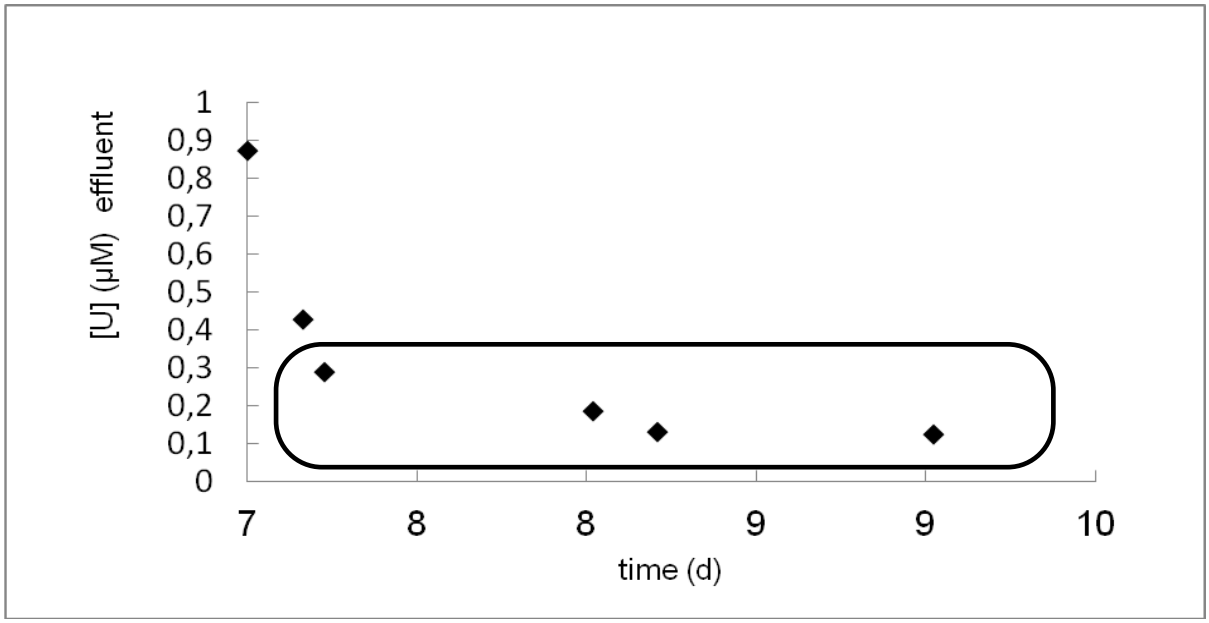

Figure 17. Example for development of CFSTR effluent uranium concentrations over time after setting the flow rate to 0.6 mL/min. Steady state is approached after 0.5 days. In this case, the last four data-points were used to calculate average steady-state net dissolution rates. Ambient pCO_2; pH 7.5 (5mM MOPS). Susp. density: 100 mg/L; I =0.01M (NaCl).

Figure 18 shows steady state uranium concentrations in the CFSTR effluents as a function of flow rates. As expected, the effluent concentrations decrease with increasing flow rates and concomitantly decreasing residence time of the fluids in the reactor. Based on the residence times and effluent concentrations, dissolution rates were calculated and plotted as a function of effluent concentrations in Figure 19. The dissolution rates in batch and CFSTR experiments show good correspondence, where batch initial dissolution rates tend to be somewhat lower than CFSTR steady state dissolution rates. This observation demonstrates that initial rates in batch experiments are not dominated by the fast initial release of high affinity sites on the mineral surface.

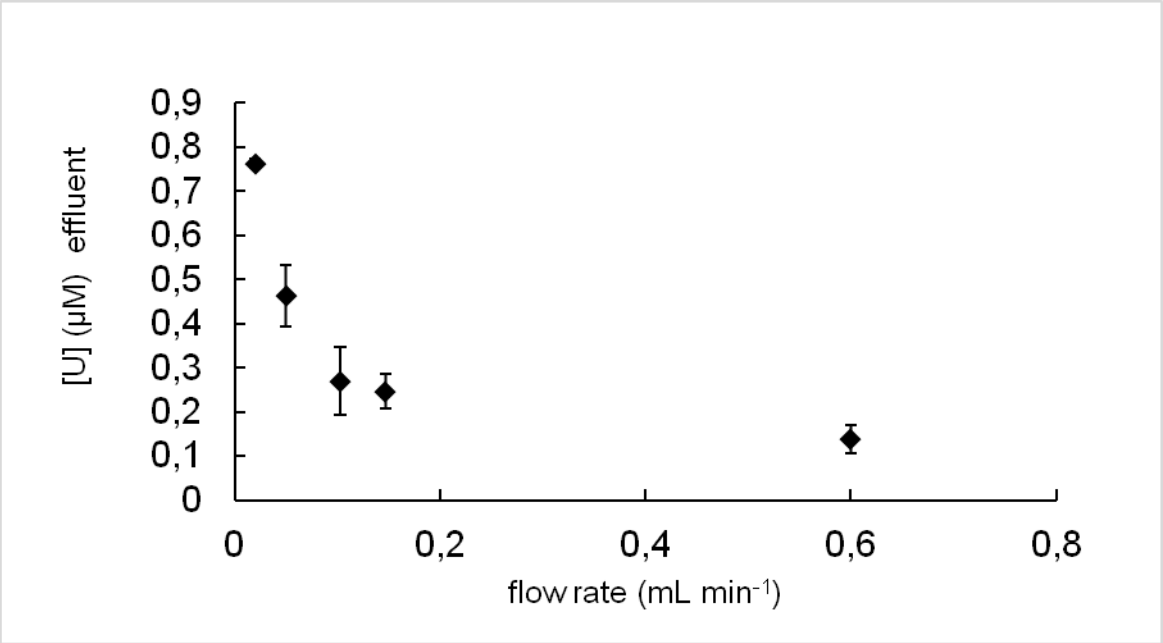

Figure 18. Average steady state uranium concentrations in the CFSTR effluent as a function of the flow rate. Error bars: +- standard deviation. Ambient pCO_2; pH 7.5 (5mM MOPS). Susp. density: 100 mg/L; I =0.01M (NaCl).

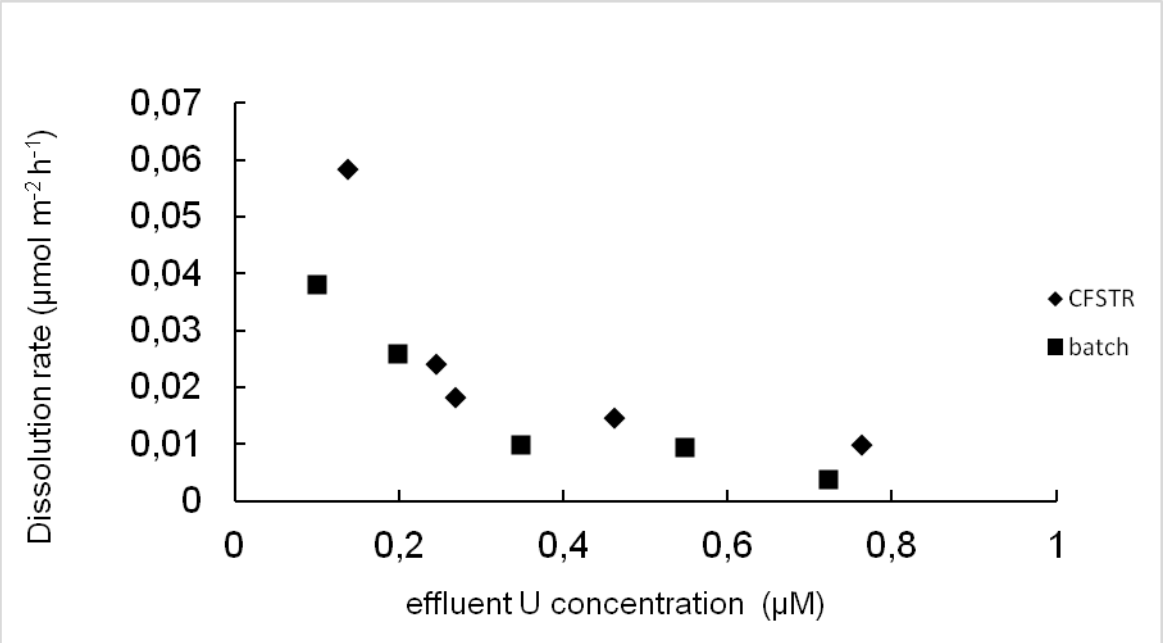

Figure 19. Dissolution rates as a function of uranium concentrations from CFSTR and batch experiments. Ambient pCO_2; pH 7.5 (5mM MOPS); Susp. density: 100 mg/L; I =0.01M (NaCl).

The effect of the solution saturation state on dissolution kinetics can be described by expressing dissolution rates as a function of the Gibbs free energy ΔG of the dissolution reaction (Kraemer and Hering 1997). ΔG is calculated by equation (9)

$$\Delta G = RT\log\left(\frac{Q}{K_{eq}}\right) \tag{9}$$

Considering the overall metaschoepite dissolution

$$UO_3(H_2O)_2 + 2H^+ \leftrightarrow UO_2^{2+} + 3H_2O \quad \text{with} \tag{10}$$

$K_{eq}=10^{5.14}$

We can calculate the ion activity quotient Q

$$Q = \left(\frac{a(UO_2^{2+})}{a(H^+)^2}\right) \tag{11}$$

From transition state theory, we can derive the following relationship between net

dissolution rates R and the maximum forward dissolution rate under far-from-equilibrium conditions R_{max}

$$R = R_{max} \cdot \left[1 - exp\left(\frac{n \cdot \Delta G}{RT}\right)\right] \quad (12)$$

where n=2

As seen Figure 20, the Gibbs free energy of reaction varies from -0.4 to -2.5 kJ/mol. This ΔG range is close to the solubility equilibrium of metaschoepite using the solubility constant of Meinrath et al (1996) (Meinrath, Kato et al. 1996). According to the TST expression above and assuming n=2 as observed for iron oxides, we would expect maximum dissolution rates at ΔG<-10 kJ/mol. This is consistent with the observation of increasing dissolution rates with decreasing ΔG as seen in Figure 20.

These calculations indicate that the solution saturation state has an effect on all dissolution experiments at pH 7.5. Considering the various influencing factors on dissolution rates as discussed in the previous section, it becomes apparent that changes in solution composition accelerating dissolution (e.g. increasing carbonate concentrations or the addition of organic ligands) may only be related with decreasing the solution saturation state of the solution with regard to the DU corrosion product and not necessarily to specific surface geochemical dissolution mechanisms such as ligand-promoted dissolution.

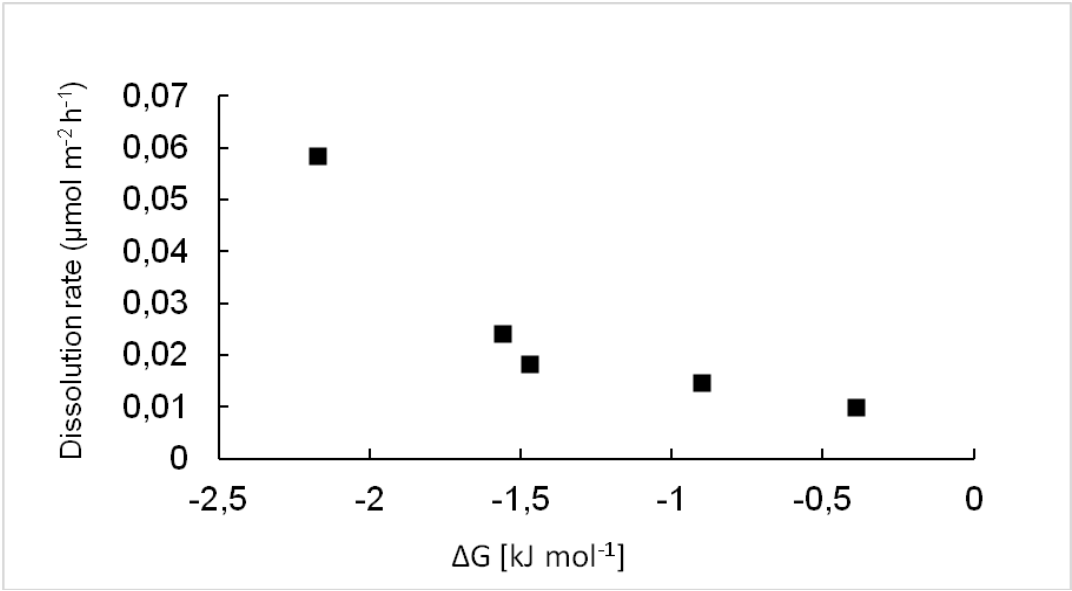

Figure 20. Effect of Gibbs free energy of reaction ΔG on dissolution rates

3.3 Impact of DU dissolution to the environment

The results show that in several batch experiments the dissolution rates vary with solution compositions, reflecting different environmental conditions. Dissolution rates are somehow affected by surface controlled dissolution mechanisms such as proton-promoted dissolution, or ligand-promoted dissolution. Solutions with low pH (proton-promoted) higher pCO2 or oxalate addition (ligand-promoted) show a dissolution accelerating effect. The initial dissolution rate is increased. At neutral pH, no CO2 the dissolution rate is reduced. Nevertheless the CFSTR run has shown that the dissolution rate is highly dependent on the solution saturation state (Figure 20). Therefore it is hard to tell whether the dissolution rate is dominated by specific surface dissolution mechanisms or the solution saturation state. This would need further investigations. However, varying solution compositions showed different effects on the dissolution rate of DU corrosion products. Therefore it is important to illustrate the impact of DU dissolution in the context of different environmental factors and the possible consequences:

The results show that a high CO_2 partial pressure enhances the dissolution rate of uranium. In the range of typical soil pH values between pH 4 and pH 9 the dissolved inorganic carbon varies more than three orders of magnitude. Considering that the pCO2 in soil gas can also vary by more than an order of magnitude depending on climate and plant activity it becomes clear that geochemical conditions such as pCO_2 can play a decisive factor influencing the dissolution of DU corrosion products (Brook, 1983). In the context of this study, it can be predicted a higher risk of mobilizing uranium through dissolution, in soils containing high carbonate concentrations. Groundwater analysis in especially carbonatic areas could be a useful task in order to determine the impact of DU to the environment and the role of dissolution in the great picture.

The effect of pH was found to be supporting on the dissolution rate of DU corrosion products under acidic (pH3-pH4.5) conditions as well as under alkaline (pH9) conditions. Factors influencing the pH of soil solution are for example bioactivity, industry (acid rain) and the soil-type. These observations of systematically changing dissolution rates as a function of pH and coupled carbonate equilibria is of significance for natural soils and aquifer materials.

Most soil pH values fall in the range between 3.5 and 9 (Slessarev, 2016). In this pH range, DU corrosion product dissolution rates vary several orders of magnitude. This may not only influence the transfer of uranium from the corrosion layer around DU penetrators to solution, but it also may affect the oxidative corrosion rates of the penetrator as it may lead to the removal of passivating layers on its surface. Carbonate soils typically have pH values in the alkaline range and may also serve as source of Ca and carbonate that are components of stable soluble uranyl-calcium-carbonate species. These conditions and acidic soil types, such as podsols, would predict a higher risk of DU release into solution. Based on our observations, the lowest dissolution rates would be expected in slightly acidic non-carbonate soils. The risk of uranium release through dissolution would be decreased there.

The ionic strength of soil solutions vary considerably depending on soil type, climate, influence of saline solutions including seawater and agricultural processes. As salinization due to irrigation is a problem in dry climates, the effect of salinization in the context of environmental risk assessments of uranium contamination from DU-ammunition should be taken into account (Rout et. al., 2015). However, such saline waters are often also characterized by elevated pH and high carbonate content, the effect of carbonate complexation and carbonate promoted dissolution may often outweigh the effect of high concentrations of electrolytes with low affinity for uranium complexation

The effect of oxalate on the dissolution of DU corrosion products was a supporting effect. Considering that carboxylic acids such as oxalate are ubiquitous in soil systems and are actively exuded by plants, fungi and microorganisms, a biogeochemical control of U(VI) mobilization from DU corrosion products is not likely, particularly in the absence of high carbonate concentrations in solution.

The organic substance content of soils and aquifer materials can vary widely. The results reported here are insufficient for elucidating the relative role of all these processes. However, it becomes clear that humic acid (HA) has a complex pH effect on dissolution of DU corrosion products. Further investigations would be needed.

4 Conclusion

In this study the dissolution of DU ammunition corrosion product was determined in batch reactors, varying solution conditions, including pH, ionic strength, CO2 partial pressure and the presence of organic ligands. The effect of the solution saturation state of uranium-hydroxides was explored in continuous flow stirred tank reactors (CFSTR).

As the results show, at equilibrium with the atmosphere (pCO2=-3.5), DU corrosion products show lowest dissolution rates at pH 6 with increasing dissolution rates towards lower and higher pH. The highest dissolution rates were found at strongly acidic pH ≤ 4.5. In the alkaline pH range we found a strong accelerating effect of increasing pCO_2 and this accelerating effect increased with pH. The observed net dissolution rates at pH 9 in the presence of a pure CO_2 atmosphere were roughly similar to rates at pH 3 at atmospheric pCO_2. Increasing concentrations of a nominally non-reactive electrolyte (NaCl) had a mildly accelerating effect on dissolution rates. The effect of a low molecular weight organic ligand (oxalic acid) with known affinity for uranyl was tested at 1mM concentrations at pH 4.5 and had a strong accelerating effect. Humic substances showed a more complex behaviour with a slightly inhibitory effect on net dissolution rates at pH 4.5 and a strongly accelerating effect (by two orders of magnitude) at pH 6.

While the results on dissolution rates summarized in the previous paragraph were measured using a batch dissolution setup, the effect of solution saturation state on net dissolution rates in a continuous flow stirred tank reactor (CFSTR) setup was investigated. In contrast to the batch setup, the CFSTR setup allows measurements of dissolution rates under constant solution saturation state conditions. We found that batch- and CFSTR-derived dissolution rates were comparable at pH 7.5. CFSTR rates and initial batch rates were all near dissolution equilibrium, with deviations in Gibbs free energies from the equilibrium state of $\Delta G \geq -2.5$ kJ/mole.

That indicates that the dissolution at pH 7.5 was fast enough to approach equilibrium rapidly. This suggests that the accelerating effect of solution composition (including effects of electrolytes, pH, pCO_2, and organic ligands) that was observed in this study may in part be due to changing solution saturation states. Disentangling the effects of ΔG and the potential effect of dissolution mechanisms such as ligand-controlled-, alkaline- and proton promoted dissolution would require further careful work. However, this finding also illustrates that in porous media, particularly under unsaturated conditions, the transport of dissolution products away from the localized DU corrosion product is likely of higher importance for the mobilization of uranium in soil water than the dissolution rate, even under conditions where dissolution is relatively slow (e.g. at pH 7.5 and atmospheric pCO_2). Generally, among rates of dissolution and rates of transport, the slower process is rate determining. We expect that under conditions where dissolution rates are faster than at pH 7.5 in the presence of ambient air (i.e. under most other conditions), the potential for transport control of uranyl mobilization from DU corrosion products in soils will be even more pronounced except maybe under high flow conditions.

5 References

Bem, H., & Bou-Rabee, F. (2004). Environmental and health consequences of depleted uranium use in the 1991 Gulf War. *Environment International Vol.30 (1)*.

Biber, M. V. (1994). The coordination chemistry of weathering: IV. Inhibition of the dissolution of oxide minerals. *Geochimica et Cosmochimica Acta 54 (9)*.

Bleise, A., Danesi, P., & Burkart, W. (2003). Properties, use and health effects of depleted uranium (DU): a general overview. *Journal of Environmental Radioactivity*.

Bone, S. E. (2017). Uranium (IV) adsorption by natural organic matter in anoxic sediments. *Proceedings of the National Academy of Sciences 114 (4)*.

Brook, G. A. (1983). A world model of soil carbon dioxide. *Earth Surface Processes and Landforms*.

Burns, P. C. (2002). The structures of becquerelite and Sr-exchanged becquerelite. *American Mineralogist 87 (4)*.

Casas I., D. P. (1998). The role of pe, pH, and carbonate on the solubility of UO2 and uraninite under nominally reducing conditions. *Geochimica et Cosmochimica Acta*.

Crea, F. A. (2007). Dioxouranium (VI)–carboxylate complexes: A calorimetric and potentiometric investigation of interaction with oxalate at infinite dilution and in NaCl aqueous solution at I= 1.0 molL− 1 and T= 25° C. *Talanta 71 (2)*.

De Pablo, J. I. (1999). The oxidative dissolution mechanism of uranium dioxide. I. The effect of temperature in hydrogen carbonate medium. *Geochimica et Cosmochimica Acta 63 (19)*.

Degueldre, C. a. (2014). Ground water colloid properties from the Bangombé system. *Applied Geochemistry*.

Dublet, G. J. (2017). Partitioning of uranyl between ferrihydrite and humic substances at acidic and circum-neutral pH. *Geochimica et Cosmochimica Acta 215*.

Fomina, M. (2008). Role of fungi in the biogeochemical fate of depleted uranium.

Furrer, G. a. (1986). The coordination chemistry of weathering: I. Dissolution kinetics of δ-Al2O3 and BeO. *Geochimica and Cosmochimica Acta*.

Giammar, D.E. (2001). GEOCHEMISTRY OF URANIUM AT MINERAL-WATER INTERFACES: RATES OF SORPTION-DESORPTION AND DISSOLUTION-PRECIPITATION REACTIONS. In *Dissertation.*

Giammar, D. E. (2002). Equilibrium and kinetic aspects of soddyite dissolution and secondary phase precipitation in aqueous suspension. *Geochimica and Cosmochimica Acta*.

Giammar, D. E. (2004). Influence of dissolved sodium and cesium on uranyl oxide hydrate solubility. *Environmental science & technology 38 (1)*.

Gorman-Lewis, D. P. (2008). Review of uranyl mineral solubility measurements. *The Journal of Chemical Thermodynamics*.

Gudavalli, R. K. (2013). Comparison of the kinetic rate law parameters for the dissolution of natural and synthetic autunite in the presence of aqueous bicarbonate ions. *Chemical Geology*.

Guillaumont, R. a. (2003). Update on the chemical thermodynamics of uranium, neptunium, plutonium, americium and technetium.

Handley-Sidhu, S. N.-R. (2009). Corrosion and transport of depleted uranium in sand-rich environments. *Chemosphere 77(10)*.

Handley-Sidhu, S. P.-R. (2008). Corrosion and fate of depleted uranium penetrators under progressively anaerobic conditions in estuarine sediment. *Environmental science & technology 43 (2)*.

Heister, K. (2014). The measurement of the specific surface area of soils by gas and polar liquid adsorption methods—Limitations and potentials.

Hummel, W. (1998). The Influence of Organic Ligands on Trace Metal Speciation. *Mineralogical Magazine*.

Ilton, E. S. (2006). The dissolution of synthetic Na-boltwoodite in sodium carbonate solutions. *Geochimica et Cosmochimica Acta 70 (19)*.

Jiang, G.-T., & Aschner, M. (2015). Depleted Uranium. In *Handbook of Toxicology of Chemical Warfare Agents.*

Kraemer, S. M. (1997). Influence of solution saturation state on the kinetics of ligand-controlled dissolution of oxide phases. *Geochimica and Cosmochimica Acta*.

Larry S. Keith, O. M. (2015). Uranium. In *Handbook on the Toxicology of Metals (Fourth Edition).*

Li,W.C., DM Victor, CL Chakrabarti (1980). Effect of pH and uranium concentration on interaction of uranium(VI) and uranium(IV) with organic ligands in aqueous solutions. *Analytical Chemistry*.

Liu, C. J. (2004). Dissolution of uranyl microprecipitates in subsurface sediments at Hanford Site, USA. *Geochimica and Cosmochimica Acta 68 (22)*.

Lovley, D. R. (1992). Bioremediation of uranium contamination. *Environ. Sci. Technol. 26*.

Meinrath, G. Y. (1996). Solid-aqueous phase equilibria of uranium (VI) under ambient conditions. *Radiochimica Acta 75 (3)*.

Papastefanou, C. (2002). Depleted uranium in military conflicts and the impact on the environment. *Health Physiks 83 (2)*.

Pérez, I. I. (1996). Dissolution studies of soddyite as a long-term analogue of the oxidative alteration of the spent nuclear fuel matrix. *MRS Online Proceeding Library Archive 465*.

Pérez, I. I. (2000). The thermodynamics and kinetics of uranophane dissolution in bicarbonate test solutions. *Geochimica and Cosmochimica Acta 64(4)*.

Reinoso-Maset, E. C. (2017). Rates and mechanisms of uranyl oxyhydroxide mineral dissolution. *Geochimica and Cosmochimica Acta 207*.

Riba, O., Walker, C., & Ragnarsdottir, K. V. (2005). Kinetic studies of synthetic metaschoepite under acidic conditions in batch and flow experiments. *Environmental science & technology 39 (20)*.

Roelofs, F. J. (2007). Solubility kinetics of a synthetic uranium (VI) oxide at different pH and controlled O2 partial pressure and evaluation of substantial interface properties. *Radiochimica Acta 95 (7)*.

Rout, S., Ravi, P., Kumar, A., & Tripathi, R. (2015). Study on speciation and salinity-induced mobility of uranium from soil. *Environmental Earth Sciences 74 (3)*.

Steward, S., E. Mones (1996). Comparison and modeling of aqueous dissolution rates of various uranium oxides.

Schindler, M. A. (2004). Prediction of crystal morphology of complex uranyl-sheet minerals. I. Theory 42 (2). *The Canadian Mineralogist*.

Slessarev, E. Y. (2016). Water balance creates a threshold in soil pH at the global scale. *Nature 540 (7634)*.

Sowder, A. S. (2001). The impact of mineralogy in the U (VI)—Ca—PO4 system on the environmental availability of uranium. *Journal of Radioanalytical and nuclear chemistry 248 (3)*.

Ulrich, K.-U. A.-L. (2008). Dissolution of biogenic and synthetic UO2 under varied reducing conditions. *Environmental science & technology*.

Vallet, V. H. (2003). Structure and bonding in solution of dioxouranium (VI) oxalate complexes: Isomers and intramolecular ligand exchange. *Inorganic Chemistry 42 (6)*.

Vermeer, A. W. (1998). Adsorption of humic acid to mineral particles. 1. Specific and electrostatic interactions. *Langmuir 14 (10)*.

Wang, G. W.-M. (2017). Uranium Release from Acidic Weathered Hanford Sediments: Single-Pass Flow-Through and Column Experiments. *Environmental science and Technology*.

Wang, Y. H.-L. (2016). Products of in situ corrosion of depleted uranium ammunition in bosnia and herzegovina. *Environmental science and Technology 50 (22)*.

Wang, Y. M.-L. (2013). Mobile uranium(IV)-bearing colloids in a mining-impacted wetland. *Nature Communication*.

Wang, Z. B. (2014). Effects of Mn (II) on UO2 dissolution under anoxic and oxic conditions. *Environmental science & technology*.

WHO. (2001). Depleted uranium: sources, exposure and health effects.

Wieland, E. B. (1988). The coordination chemistry of weathering: III. A generalization on the dissolution rates of minerals. *Geochimica and Cosmochimica Acta*.

Yoon, T. H. (2005). Adsorption of organic matter at mineral/water interfaces. IV. Adsorption of humic substances at boehmite/water interfaces and impact on boehmite dissolution. *Langmuir 21 (11)*.

6 Appendix

Dates corresponding to Figure 8

time	[U] (µM) CO2 free ph7.5	Std.dev CO2 free ph 7.5	[U] (µM) pCO2=-3.5 ph 7.5	Std.dev pCO2=-3.5 ph 7.5	[U] (µM) pCO2=0 ph 7.5	Std.dev pCO2=0 ph 7.5
0,25	0,059464	0,01895	0,077718	0,010713	52,96711	7,82068
0,5	0,070584	0,009669	0,070642	0,01813	74,77166	7,642752
1	0,072814	0,013782	0,090169	0,013866	138,8076	8,475866
2	0,095774	0,015719	0,136494	0,049677	177,2887	2,518497
4	0,118752	0,016567	0,143963	0,036768	204,8147	1,397943
8	0,127376	0,024761	0,278757	0,110831	215,9342	1,040252
24	0,126694	0,031116	0,432383	0,133641	228,8132	0,181356
48	0,094203	0,024197	0,650728	0,15051	233,7622	4,793355
96	0,068917	0,012526	0,823268	0,296678	231,742	9,260917
192	0,083029	0,012	0,831479	0,051859	241,6612	0,659328

Dates corresponding to Figure 9

time	[U] (µM) CO_2 free ph 9	Std.dev. CO_2 free ph 9	[U] (µM) pCO_2=-3.5 ph 9	Std.dev. pCO_2=-3.5 ph 9	[U] (µM) pCO_2=0 ph 9	Std.dev. pCO_2=0 ph 9
0,25	0,088283	0,03624	0,33399	0,055488	32,90929	0,695098
0,5	0,10883	0,052912	0,43499	0,028541	43,17527	1,240873
1	0,126196	0,039865	0,692506	0,033358	78,24342	3,509336
2	0,163105	0,043678	1,20768	0,150478	135,6471	16,64132
4	0,276838	0,045492	2,198525	0,287232	187,4137	13,34059
8	0,309136	0,012712	3,555828	0,366899	224,901	32,76349
24	0,39214	0,02527	9,211385	2,191563	255,1316	24,06653
48	0,353777	0,006124	15,70173	2,34703	281,6431	15,0908
96	0,360538	0,02939	22,57872	2,418917	281,7885	7,591873
192	0,376724	0,043123	30,7475	2,850376	295,4456	10,98428

Dates corresponding to Figure 10

time	[U] (µM) ph3	Std.dev. ph 3	[U] (µM) ph 4.5	Std.dev. ph 4.5	[U] (µM) ph 6	Std.dev. ph 6	[U] (µM) ph 7.5	Std.dev. ph 7.5	[U] (µM) ph 9	Std.dev. ph 9
0,25	24,311	1,690	0,126	0,064	0,102	0,027	0,078	0,011	0,334	0,055
0,5	36,738	2,239	0,130	0,031	0,105	0,022	0,071	0,018	0,435	0,029
1	63,213	0,741	0,228	0,162	0,136	0,050	0,090	0,014	0,693	0,033
2	93,715	9,314	0,536	0,487	0,182	0,034	0,136	0,050	1,208	0,150
4	133,434	5,143	0,638	0,284	0,206	0,014	0,144	0,037	2,199	0,287
8	159,943	0,827	4,591	1,852	0,175	0,022	0,279	0,111	3,556	0,367
24	183,451	5,259	52,562	11,114	0,316	0,095	0,432	0,134	9,211	2,192
48	185,217	12,137	82,532	3,051	0,465	0,010	0,651	0,151	15,702	2,347
96	186,395	12,750	125,228	22,795	0,511	0,175	0,823	0,297	22,579	2,419
192	201,347	12,104	134,643	23,969	0,660	0,519	0,831	0,052	30,748	2,850

Dates corresponding to figure 11

pH	experiment	model
3	0,000189076	
4,5	0,00012605	4,60E-04
6	6,30252E-07	3,00E-06
7,5	8,40336E-07	1,14E-06
9	3,36134E-05	5,00E-05

Dates corresponding to figure 12

time	[U] (µM) NaCl 10mM ph 7.5	Std.dev. NaCl 10mM ph 7.5	[U] (µM) NaCl 30mM ph 7.5	Std.dev. NaCl 30mM ph 7.5	[U] (µM) NaCl 100mM ph 7.5	Std.dev. NaCl 100mM ph 7.5
0,25	0,078	0,011	0,137	0,023	0,278	0,007
0,5	0,071	0,018	0,177	0,030	0,391	0,093
1	0,090	0,014	0,254	0,052	0,510	0,095
2	0,136	0,050	0,333	0,014	0,681	0,065
4	0,144	0,037	0,543	0,118	0,714	0,100
8	0,279	0,111	0,909	0,319	1,328	0,156
24	0,432	0,134	1,127	0,104	1,725	0,323
48	0,651	0,151	2,091	0,783	2,943	0,280
96	0,823	0,297	2,750	0,777	3,553	0,059
192	0,831	0,052	2,972	0,152	4,818	0,511

Dates corresponding to figure 13

experimental data; [U] (M)	modelled data ; [U] (M)	TIC
8,40336E-07	0,00000114	1,80E-04
2,97198E-06	1,64E-06	1,94E-04
4,81767E-06	5,12E-06	2,23E-04

Dates corresponding to figure 15

time	[U] (µM) oxalate 1mM ph 4.5	Std.dev. oxalate 1mM ph 4.5	[U] (µM) no oxalate ph 4.5	Std.dev. no oxalate ph 4.5
0,25	18,790	6,992	0,126	0,064
0,5	28,457	13,367	0,130	0,031
1	46,787	17,565	0,228	0,162
2	73,311	29,917	0,536	0,487
4	110,922	23,566	0,638	0,284
8	149,823	21,686	4,591	1,852
24	169,468	16,330	52,562	11,114
48	198,106	33,885	82,532	3,051
96	197,642	18,120	125,228	22,795
192	218,458	28,567	134,643	23,969

Dates corresponding to figure 16

time	[U] (µM) humic acid ph 4.5	Std.dev. ph 4.5	[U] (µM) humic acid ph 6	Std.dev. ph 6	[U] (µM) no humic acid ph 4.5	Std.dev. ph 4.5	[U] (µM) no humic acid ph 6	Std.dev. ph 6
0,25	1,205	1,077	0,583	0,179	0,126	0,064	0,102	0,027
0,5	2,033	1,262	0,954	0,231	0,130	0,031	0,105	0,022
1	3,048	1,630	1,564	0,311	0,228	0,162	0,136	0,050
2	4,635	2,248	2,431	0,500	0,536	0,487	0,182	0,034
4	6,224	2,191	3,455	0,517	0,638	0,284	0,206	0,014
8	9,194	3,400	4,716	0,347	4,591	1,852	0,175	0,022
24	16,332	3,213	7,973	0,330	52,562	11,114	0,316	0,095
48	24,360	7,326	11,250	1,949	82,532	3,051	0,465	0,010
96	27,120	5,024	14,586	0,245	125,228	22,795	0,511	0,175
192	38,357	4,823	17,294	0,815	134,643	23,969	0,660	0,519

Dates corresponding to figure 17

time (days)	dissolution rate	[U](µM)	flow rate (ml/min)
0,042	0,018	0,098	0,280
0,125	0,075	0,400	0,280
0,208	0,083	0,443	0,280
0,896	0,070	0,346	0,302
0,958	0,068	0,334	0,302
1,042	0,068	0,335	0,302
1,125	0,064	0,311	0,308
1,188	0,061	0,301	0,304
2,063	0,088	0,447	0,294
3,063	0,057	0,300	0,282
4,063	0,045	0,231	0,292
7,000	0,171	0,873	0,292
7,167	0,190	0,426	0,663
7,229	0,120	0,289	0,616
8,021	0,077	0,185	0,620
8,208	0,054	0,132	0,616
9,021	0,053	0,123	0,640
10,021	0,049	0,113	0,640
13,031		0,476	0,147
14,062		0,462	0,144
15,104		0,462	0,145
15,812	0,026	0,273	0,144
18,958	0,027	0,280	0,144
19,979		0,192	0,146
21,896		0,240	0,147
22,937		0,293	0,103
25,937	0,022	0,330	0,100
26,812	0,023	0,340	0,102
27,896		0,199	0,098
29,937		0,206	0,101
32,812		0,439	0,047
33,854	0,015	0,491	0,047
34,875	0,016	0,528	0,046
36,896		0,467	0,047
39,958		0,366	0,049
42,917		0,582	0,019
46,937	0,010	0,756	0,019
47,937	0,010	0,757	0,020
48,937	0,009	0,760	0,019
49,937	0,010	0,778	0,019

Dates corresponding to figure 18

flow rate (ml/min)	effluent [U] (µM)
0,144	0,273
0,144	0,280
0,1	0,330
0,102	0,340
0,047	0,491
0,046	0,528
0,0189	0,756
0,02	0,757
0,0185	0,760
0,0192	0,778
0,616	0,132
0,64	0,123
0,64	0,113
0,302	0,334
0,302	0,335
0,308	0,311

Dates corresponding to figure 19

[U] (µM) CFSTR	dissolution rate µmol m-2 h-1 CFSTR	[U] (µM) batch pH 7.5	dissolution rate µmol m-2 h-1 batch pH 7.5
0,273	0,026	0,100	0,038
0,280	0,027	0,200	0,026
0,330	0,022	0,349	0,010
0,340	0,023	0,549	0,009
0,491	0,015	0,723	0,004
0,528	0,016		
0,756	0,010		
0,757	0,010		
0,760	0,009		
0,778	0,010		
0,132	0,051		
0,123	0,050		
0,113	0,043		

Dates corresponding to figure 20

[U] (µM) batch pH 7.5	dissolution rate µmol m-2 h-1 batch pH 7.5
0,100	0,038
0,200	0,026
0,349	0,010
0,549	0,009
0,723	0,004

Zusammenfassung

Abgereichertes Uran wird aufgrund dessen physikalischen Eigenschaften (hohe Dichte, selbst entzündlich) als Munition in militärischen Konflikten genutzt. Bis zu 90% der Munition trifft nicht und wird daher größtenteils in die Umwelt verstreut. Verschiedene Verwitterungsprozesse wie Korrosion, Auflösung und Transport zersetzen das Material und sorgen so für einen Uran-Eintrag in die Umwelt. Diese Arbeit beschäftigt sich mit dem Auflösungsprozess des bereits korrodierten Materials der Munition. Dabei wurden zwei verschiedene Experimente durchgeführt. Zum einen wurde in Batch-Experimenten die Auflösung des korrodierten Urans in verschiedenen Lösungen getestet. Die Abhängigkeit von Umweltrelevanten Eigenschaften wie pH, Salzgehalt, Partialdruck von CO_2 sowie der Zugabe von zwei organischen Liganden Oxal-säure und Humin-säure wurden untersucht. Die Ergebnisse zeigen eine Zunahme der Löslichkeitsrate in saurem (pH 3- pH 4.5) und alkalinem (pH 9) Milieu. Die Erhöhung des CO2-Partialdrucks und die Zugabe von Oxalsäure hatten ebenso eine steigernde Wirkung auf die Löslichkeitsrate. In dem zweiten Versuchsaufbau (CFSTR) wurde getestet inwieweit der Sättigungsstatus der Lösung eine Rolle auf die Löslichkeitsrate hat. Es wurde bei einem pH von 7.5 festgestellt je höher der Sättigungsstatus der Lösung ist, desto kleiner ist die Löslichkeitsrate. Diese Erkenntnisse könnte man beispielsweise dazu nutzen, das Vermögen eines Bodentyps, Uran aufzulösen aufgrund dessen geochemischen Eigenschaften, einzuschätzen.

Abstract

Depleted uranium (DU) is used in modern military conflicts as an ammunition. Most of the munition (90%) miss their targets and bury themselves in the ground, where the DU material is subjected to several weathering processes. Corrosion, dissolution and transport are the main processes controlling the mobility of the DU corrosion product and its potential impact to the environment. This thesis focuses on the dissolution process of the DU corrosion products. Two experimental set-ups have been performed. In batch experiments, the effect of different environmental conditions such as pH, pCO_2, salinity and organic ligands on the dissolution of DU have been tested. The results show that dissolution rate is increased at both acidic- (pH 3-4.5) and alkaline (pH 9) conditions. High CO_2 partial pressure as well as oxalic acid showed strongly supporting effects on the dissolution rate of uranium. The second experiment was performed using a continuous-flow stirred-tank reactor set-up in which dissolution products are removed from the system and the influence of the solution saturation state on the dissolution rate can be determined. The results show that the dissolution rate of DU is influenced by the solution saturation state. Increased solution saturation state has led to a slowdown of the dissolution rate. In summary, the dissolution of DU corrosion products was shown to be dependent on varying environmental parameters. These findings could be used for risk assessment in order to identify and distinguish risky soil from unproblematic soils in the context of DU dissolution.